The International Journal of Advanced Manufacturing Technology (2022) 121:1533–1574
https://doi.org/10.1007/s00170-022-09051-0

CRITICAL REVIEW

A review of simulation and experiment research on cutting mechanism and cutting force in nanocutting process

Dongju Chen[1] · Shuiyuan Wu[1] · Yazhong He[1] · Yuchi Luo[2] · Xiang Wang[3]

Received: 29 September 2021 / Accepted: 12 March 2022 / Published online: 16 June 2022

Abstract
Nanocutting is a method of direct machining in nanomanufacturing field, and it is an important ultraprecision machining method. Nanocutting technology adopts single-point diamond cutting and nanoprobe scratching methods to make the machining accuracy of parts reach the nanometric scale. It is the method with the highest machining accuracy at present, so it is widely used in the processing of precision components. At the same time, nanocutting technology can be used to process nanostructures and provide processing methods for basic research in condensed matter physics. This paper summarized the cutting mechanism and cutting force in the nanocutting process, including the mechanism of nanocutting and brittle–ductile transition. The influence of RTS, temperature, wear and subsurface phase transformation on cutting performance is also discussed. At the same time, the characteristics of cutting force and friction coefficient during the cutting process are reviewed. After that, the simulation and experiment research of the nanocutting process are analyzed. At the end of the paper, the challenges and prospects of nanocutting technology are proposed and summarized.

Keyword Nanomanufacturing · Cutting · Wear · Subsurface · Experiment

1 Introduction

The manufacturing industry has gradually shifted from macroscopic manufacturing to microscopic manufacturing, especially nanomanufacturing [1–3]. Nanomanufacturing technology is a technology with material removal depth at the atomic level, and it is an ultraprecision machining method and has a wide range of applications in various fields such as aviation, energy, optics and electronics, which shows highly important practical value [4–7]. The applications of nanomanufacturing technology are listed in Table 1.

Nanomanufacturing technology can be used in two manufacturing processes. One is to manufacture nanostructures, and the other is to manufacture surface of parts with nanoscale precision [18]. Figure 1 shows the nanostructures used for communication [19–21].

In the nanomanufacturing process of nanostructures, the use of scanning probe microscope (SPM) to machine the surface of the workpiece is a common method. The scanning probe microscope realizes the manufacture of nanostructures by moving the probe in three coordinate directions, as shown in Fig. 2 [9].

At the same time, ultraprecision machining tools adopting the method of single-point diamond turning can also achieve nanomachining accuracy. In 1962, Union Cardie of the United States developed an ultraprecision hemispherical surface processing equipment, which can process aluminum alloy hemispherical surfaces with a diameter of 101.6 mm to a mirror effect, with a processing shape accuracy of 0.6um and a surface roughness of 25 nm, which is also the first time for mankind to achieve nanoprocessing accuracy in the cutting process. Later in the 1970s, Moore Company, Pneumo Company and Dutch Phillips Company in America also developed ultraprecision machine tools with a machining surface accuracy of 10 nm successfully, as shown in Fig. 3 [10, 23, 24, 28].

✉ Dongju Chen
djchen@bjut.edu.cn

1 Faculty of Materials and Manufacturing, Beijing University of Technology, Beijing, China

2 Institute of Nuclear Physics and Chemistry, China Academy of Engineering Physics, Mianyang, Sichuan, China

3 School of Mechanical and Electronic Engineering, Jingdezhen Ceramic Institute, Jingdezhen, Jiangxi, China

Table 1 Applications, methods and accuracy of nanomanufacturing technology

Authors Organizations	Applications	Method	Accuracy
Li et al. [8]	Negative index metamaterials	Nanoimprinting	P = 850 nm
Mao et al. [9]	3D nanostructures	SPM machining	Height = 60 nm
Union Cardie [10]	Hemispherical surface	Ultraprecision machining tools	Roughness = 25 nm
Moore Company, Pneumo Company and Dutch Phillips Company [10]	Mechanical parts	Ultraprecision machining tools	Roughness = 10 nm
Emboras et al. [11]	Atomic-scale plasmonic switch	Application of a positive voltage	Dimension = 1 atom
Feng et al. [12]	2D materials	Electrochemical reaction	Dimension = 1 atom
Park et al. [13]	2D materials	Atomic-scale etching	Depth = 16 Å
Yan et al. [14]	Nanochannels	AFM nanoscratching	Depth = 203 nm
Huang et al. [15]	Nano-pattern	AFM machining	Depth = 2.5 nm
Dong et al. [16]	Nanostructures	Focused ion beam	Size = 10 nm
Tseng et al. [17]	Nanoconstrictions	AFM machining	Height = 20 nm

2 Cutting mechanism

The research on nanocutting mechanism is the theoretical basis for realizing nanocutting. In the nanocutting process, not all materials within the cutting thickness range are removed. When the ratio of the cutting thickness to the cutting edge radius is less than the critical value, no chips will be generated during the cutting process, as shown in Fig. 4. The use of plastic cutting for brittle materials is also an important research direction of nanocutting mechanism. Through the nanocutting method, the processing of brittle materials can be realized. The reason is that in the cutting process of brittle materials, when the cutting thickness reaches nanometric level, the cutting mode will change from brittle mode to plastic mode, so as to realize the plastic processing of brittle materials. In this process, the most important thing is to determine the critical depth of cut in order to realize the brittle–plastic transformation of material processing [11]. The results of researches on the nanocutting mechanism are summarized in Table 2.

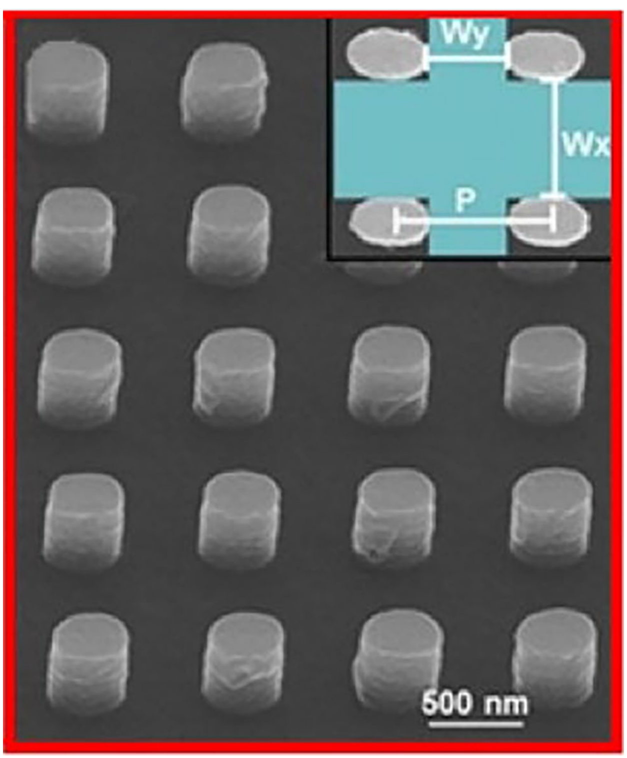

Fig. 1 Nanomanufacturing examples [8, 19, 22]

In the nanocutting process, the ratio of cutting depth to cutting edge radius can be defined as the relative sharpness of the tool RTS, and RTS = h_0/r_e, where h_0 represents the cutting depth and r_e represents the cutting edge radius. The cutting model with the same RTS and different cutting edge radius is shown in Fig. 5. It can be found that when the RTS is the same, the reduction in the cutting edge radius leads to the reduction in the cutting depth. At the same time, during the cutting process, the plastic deformation flow is formed in the area of the workpiece near the rake face of the tool, which becomes the primary deformation zone (PDZ). By increasing the depth of cut, when the RTS is unchanged, the PDZ area will also increase and will lead to an increase in internal defects of the workpiece [37, 38].

In the processing of brittle materials, in order to obtain the critical cutting depth of brittle–plastic transition, taper cutting experiments are often used to obtain this critical value. In the taper cutting experiment, as the cutting depth increases, the cutting surface gradually becomes rough and generates a lot of chips. The surface cutting process begins to change to brittle cutting mode, and the cutting depth from plastic cutting to brittle cutting is the critical depth of cut for brittle–plastic transition, as shown in Fig. 6 [19].

Nanoscratch experiment is also a kind of method of taper cutting. In the process of nanoscratch, the cutting depth is also increasing with the increase in normal load and cutting

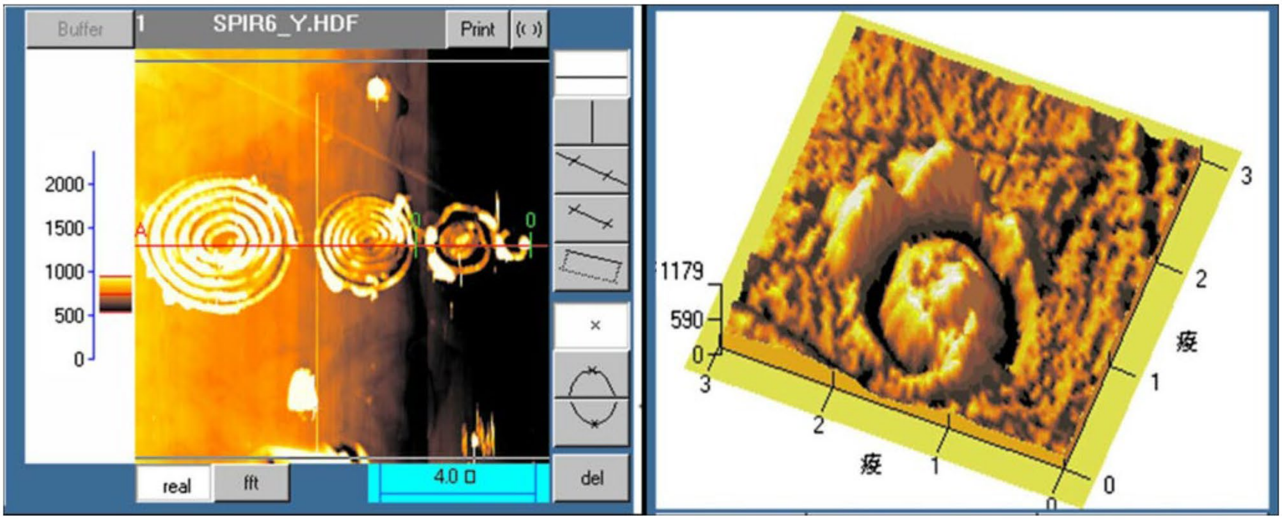

Fig. 2 (Color online) (**a**) Machining patterns by cutting at varying pitches. (**b**) Very dense spiral cuts [9]

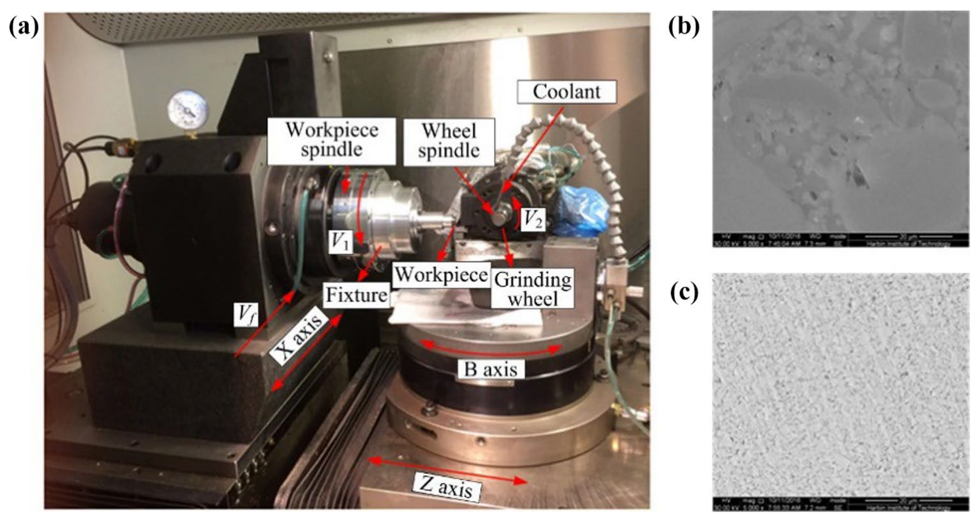

Fig. 3 Ultraprecision grinding: (**a**) ultra-precision grinding system, (**b**) and (**c**) workpiece surface morphology after ultra-precision grinding [23]

displacement, and the whole cutting process is divided into four stages. At the beginning, it is the elastic stage, followed by the elastic–plastic stage, plastic stage and brittle stage, and once it enters the brittle stage, the cutting force decreases because the material is removed in a brittle way, as shown in Fig. 7 [31].

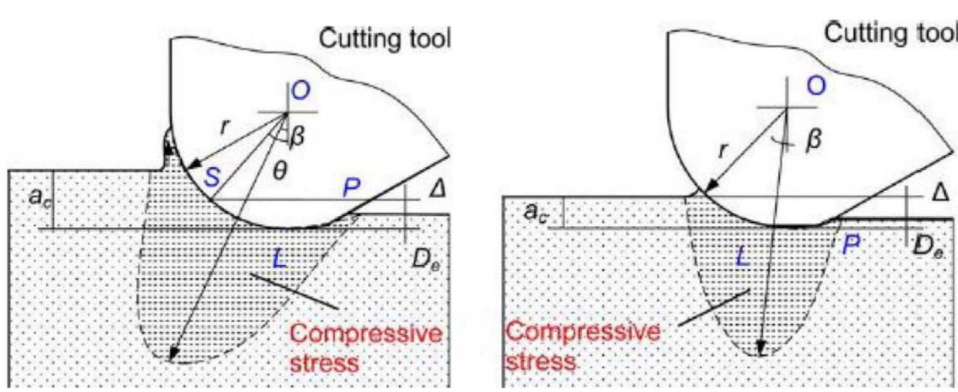

Fig. 4 Stagnation point denoted by "S" in nanocutting. The stagnation point is where the split flow of material occurs (left). For an extreme small cutting depth (right), there is no chip formation [19]

Table 2 Cutting mechanism in nanocutting process

Authors	Methods	Research factors	Results
Seyed et al. [9]	Nanomachining	Ratio of cutting depth to cutting edge radius	Small or large chip formation and stress formation
Fang et al. [25]	Nanomachining	Ratio of cutting thickness to cutting edge radius	Chip formation or no chip formation
Leung et al. [26] Wang et al. [27]	Nanoscratch test	Scratching depth	Ductile or brittle cutting
Liu et al. [29]	Nanoscratch test	Temperature Scratching depth	Ductile or brittle cutting
Kovalchenko [31]	Molecular dynamics	Cutting edge radius	Ductile or brittle cutting
Wang et al. [36]	Molecular dynamics	Ratio of depth of cut to radius, depth of cut	Material removal by extrusion and shear

In the processing of soft and brittle materials, such as KDP crystals, plastic cutting of brittle materials can be achieved by reducing the cutting depth to a few nanometers. However, for this ultraprecision machining method, there are still shortcomings of low cutting efficiency. At the same time, through the study of some difficult-to-machine materials such as ceramics, it is found that when the heat-assisted process is used, the processing difficulty can be significantly reduced. However, there are few studies on the plastic processing of KDP crystals using thermally assisted processes. Therefore, it is necessary to study the processing methods of soft and brittle materials such as KDP. Through the scratch test on the KDP crystal at 23 °C and 170 °C, it can be found that during the process of scratching the KDP crystal at 23 °C, a lot of debris is generated around the scratch, and the scratch is relatively rough. In the process of scratching the 170 °C KDP crystal, there is less debris around the scratch and the scratch is relatively smooth, as shown in Figs. 8, 9, 10. Through further analysis, it can be found that the critical brittle–plastic transition cutting depth (3.61um) of KDP crystal at 170 °C is 8.6 times of that at 23 °C (0.42um). This further verifies the positive influence of temperature on the plastic cutting of KDP crystals and provides experiment guidance for the study of crack-free surface processing of KDP crystals [29].

Ultraprecision machining can realize the removal of nanomaterials [54], but when the cutting depth drops to a few atoms, it is difficult to achieve by experimental methods, and the use of molecular dynamics simulation methods becomes feasible. Molecular dynamics method can simulate the cutting characteristics of different cutting conditions, cutting edge radius and cutting material when the cutting depth is a few atoms. It

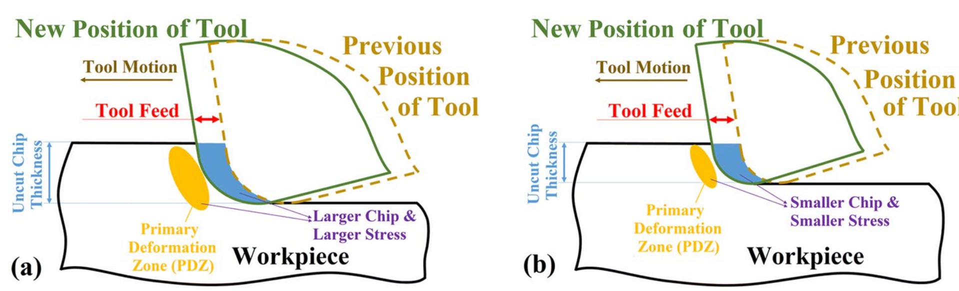

Fig. 5 The effect of tool edge radius on the machined surface at the same RTS and tool advancement, but at (**a**) higher uncut chip thickness and (**b**) lower uncut chip thickness [30]

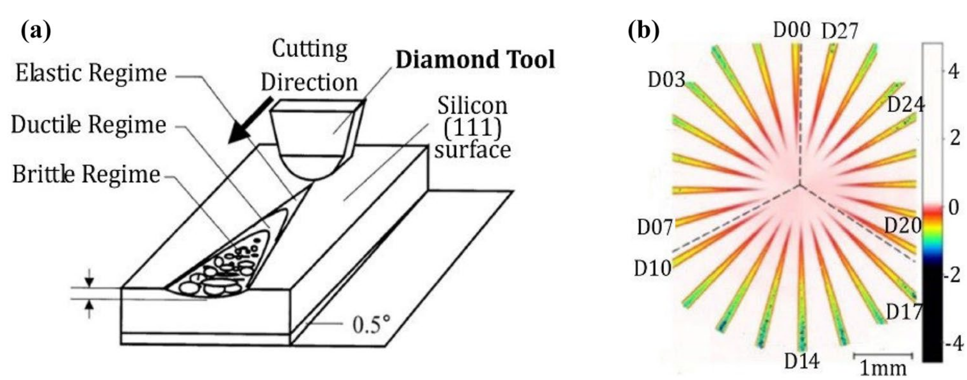

Fig. 6 Taper cutting [26] and the groves on GaF_2 single crystal [27]. The ductile–brittle transition is denoted by the onset of surface cracks as the cutting depth exceeds the critical value [19]

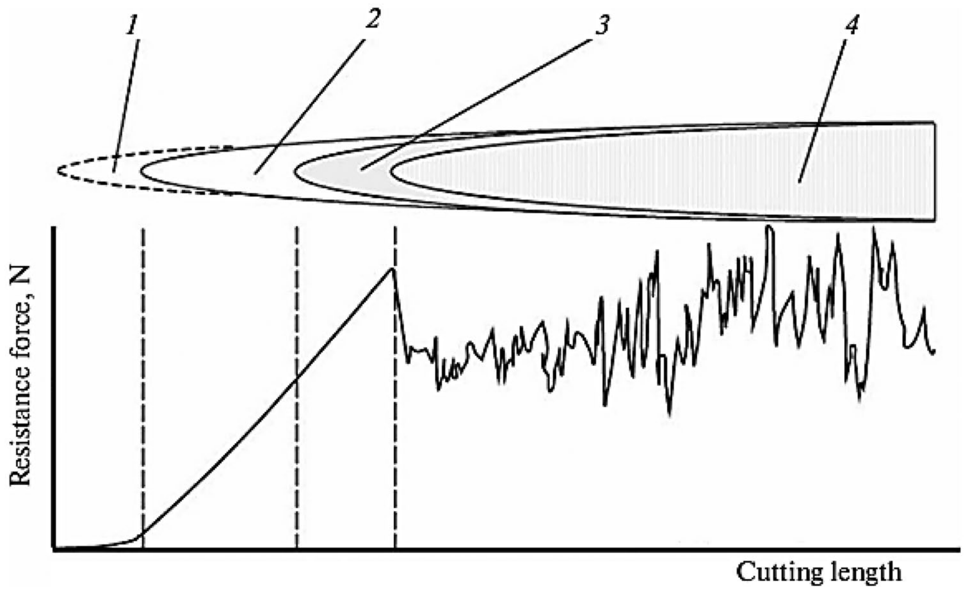

Fig. 7 Scheme of different modes of removing a brittle material with increasing normal load and cutting depth: elastic (1) and elastoplastic (2) deformations, plastic (3) and brittle (4) removal of the material [31]

is the most effective simulation method for studying nanocutting process so far [32–34]. Through the molecular dynamics simulation of the nanocutting process, the cutting stress during the cutting process can be obtained. The calculation formula of von Mises stress in nanocutting process is:

$$\sigma_{vonmises} = \sqrt{\frac{(\sigma_x - \sigma_y)^2 + (\sigma_x - \sigma_y)^2 + (\sigma_x - \sigma_y)^2 + 6(\tau_{xy}^2 + \tau_{xz}^2 + \tau_{yz}^2)}{2}}.$$

The calculation formula of hydrostatic pressure is:

$$\sigma_{hydrostatic} = \frac{\sigma_1 - \sigma_3}{2}$$

Among them, $\sigma_x, \sigma_y, \sigma_z, \tau_{xy}, \tau_{xz}$ and τ_{yz} are the six-direction stresses of a single atom and σ_1 and σ_3 are the main stresses. The equivalent von Mises stress and hydrostatic pressure of workpiece during nanocutting process are shown in Figs. 11 and 12, respectively [44].

The use of molecular dynamics simulation methods to study the mechanism of nanocutting is also an important

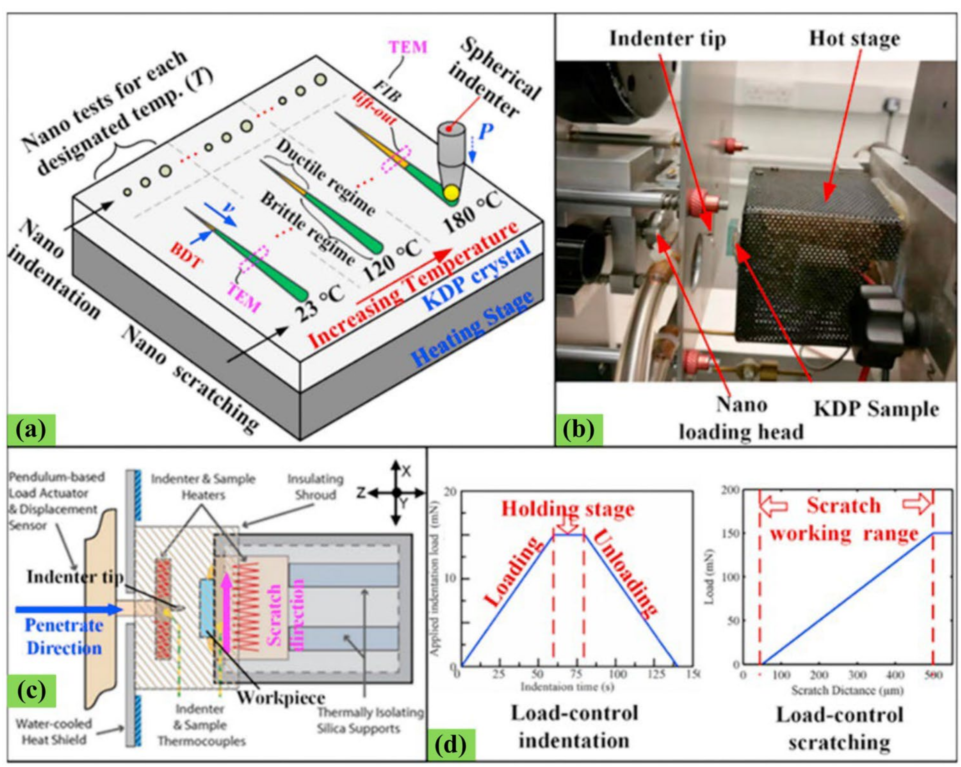

Fig. 8 (**a**) Schematics of nanotests at varying temperatures; (**b**) close snapshot of the experimental system (NanoTest); (**c**) schematic of heating arrangement of NanoTest; (**d**) diagrams of nanoindentation and scratch tests at different temperatures [29]

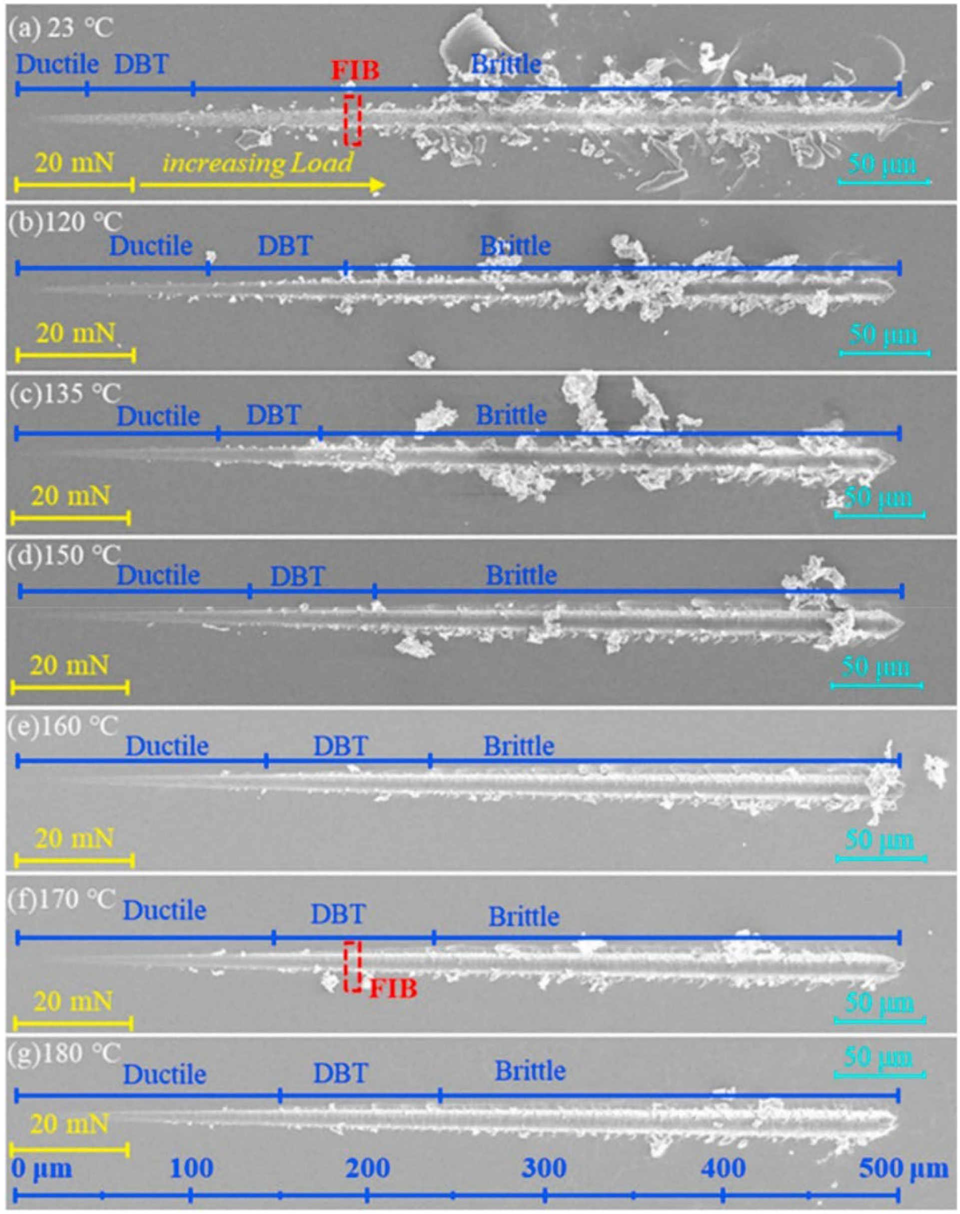

Fig. 9 The residual groove morphologies of varied-depth scratches at different temperatures [29]

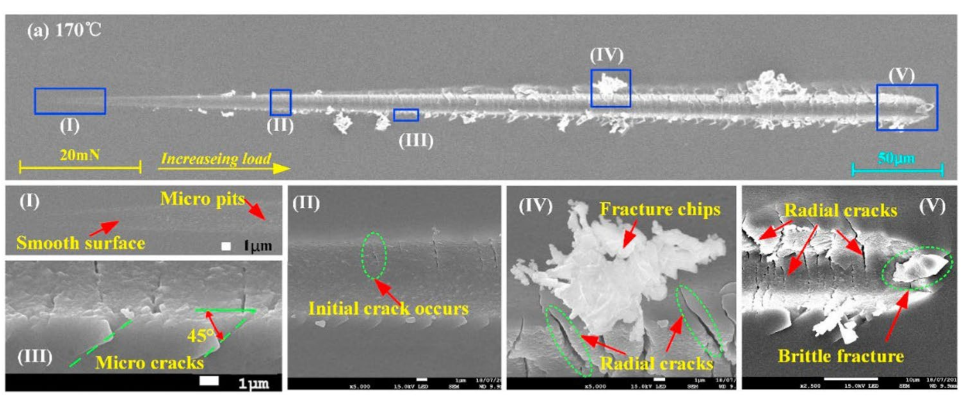

Fig. 10 The scratch surface morphologies processed at elevated temperature (e.g., 170 °C) (**a**); (I–V) are the magnified images showing the representative morphology features [29]

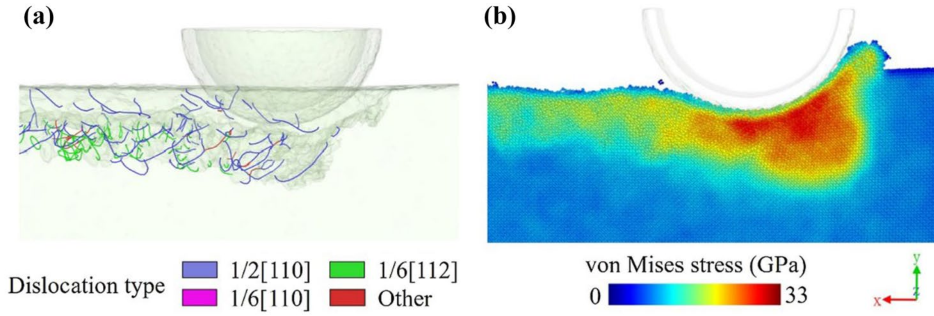

Fig. 11 **a** Dislocation distribution and **b** von Mises stress distribution in the subsurface of the nanocutting model [44]

direction. The use of the method can directly characterize the various physical and chemical interactions between the tool and the workpiece in the nanocutting process and can increase the simulation types of tools and the forms of the cutting process, such as the simulation of grinding wheels and milling tools as well as bevel cutting process. Through the molecular dynamics simulation, the cutting force and subsurface deformation as well as phase change of the workpiece during the cutting process can be obtained. At the same time, in the process of using molecular dynamics simulation, improving the simulation scale is also an important topic. At present, the use of parallel calculation method can effectively improve the simulation scale and speed. The applications of molecular dynamics simulation method for the investigation of nanocutting mechanism are shown in Table 3 [37, 47–49].

The application of molecular dynamics to simulate nanocutting process is an effective method to study the nanocutting process, but the scale of molecular dynamics simulation method has certain limits [51–53]. Usually, the model scale to study the interaction characteristics between materials is below 100 nm. The multiscale simulation method effectively solves this problem. Through the combination of molecular dynamics simulation method and finite element simulation method, a method based on quasi-continuous medium is proposed. In the quasi-continuous medium-based method, molecular dynamics simulation is used to model the key area, while finite element simulation is used to model the rest, so that the establishment and simulation of large-scale models can be realized, and then, large-scale models can be established and simulated. During the cutting process, the characteristics of cutting surface roughness, cutting force, residual stress and temperature are accurately simulated, as shown in Figs. 13 and 14 [5, 55–61, 72, 75].

Due to the anisotropy of crystalline materials, the crystal orientation has a great influence on the surface generation of the workpiece during nanocutting process [74]. Based on the slip theory, Liu [62] et al. proposed a theoretical model to analyze the influence of crystal orientation on arbitrary crystals in nanocutting process. A series of molecular dynamics (MD) simulations of nanocutting under various crystal orientations have been carried out to investigate the surface generation mechanism of the single-crystal material, as shown in Fig. 15. The simulation results show that the cutting direction determined the shape of material accumulation and the propagation direction of subsurface defects, and the width of the tool and the thickness of uncut chip determined the range of accumulation and subsurface defects [62].

Compared with traditional cutting methods, ultrasonic vibration cutting (UVC) has received more and more attention from researchers due to its advantages such as low cutting force, high cutting stability, low tool wear and good machining quality [63].

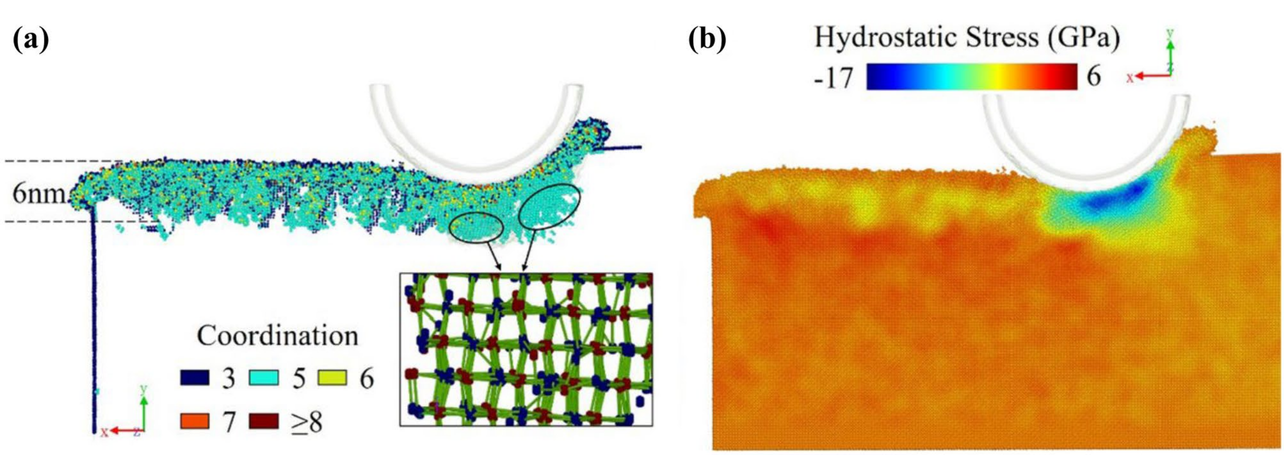

Fig. 12 Distribution of a high coordination atoms and five-coordination structure and b hydrostatic stress distribution [44]

Table 3 Nanocutting mechanism investigated by using molecular dynamics

Authors	Methods	Research factors	Results
Bai et al. [35]	MD	Rake angle of cutting tool	Better cutting performance using negative rake angle
Wang et al. [36]	MD	Fracture mechanism of brittle material	Fracture formation process, stress, cutting force, temperature
Zhou et al. [38]	MD	Structural vacancy defects	Removal mechanism, abrasion, temperature, yield stress, subsurface damage, brittle– ductility transformation based on dislocation theory
Xie et al. [39]	MD	Cutting tool edge radius	Material removal mechanism
Wang et al. [40]	MD	Cutting mechanism of amorphous alloys	Lower velocity leads to smooth machined surface
Liu et al. [41]	MD	Crystal orientations	Cutting direction influences propagating direction of subsurface defects
Wang et al. [42]	MD	Fluid Media	Deformation of workpiece is decreased, the cutting force is reduced, and the height of cutting chip and depth of subsurface damage layer are lowered; the highest and whole temperature of the workpiece is significantly reduced
Liu et al. [43]	MD	Tip radius, crystal structure evolution and subsurface defect thickness	Smaller tip radius leads to the possibility of plastic material removal, and subsurface defect thickness increases with the increase in indenter tip radius and scratching depth
Chen et al. [44]	MD	Subsurface deformation mechanism	Dislocations, phase transformation, subsurface stress
Zhu et al. [45]	MD	Elliptical vibration-assisted nanocutting	Brittle to ductile cutting mechanism, phase transformation, stress, temperature, cutting force
Zhao et al. [46]	MD	Grain and the subgrain boundaries	The grain and the subgrain boundaries lead to continuous pile-up formation, obvious stresses accumulation, elastic recovery of the machined surface and periodic oscillation of processing force

3 Tool wear

With the development of diamond cutting technology, brittle materials such as silicon and germanium can be removed by plastic cutting, but diamond tools wear fast during the machining process. Therefore, it is necessary to study the wear mechanism of the tools in the nanocutting process. Researchers have studied the wear of diamond tools with diamond cutting workpieces with different crystal orientations and found that when the rake face crystal orientation is (110), the thrust force of the tool is smaller, so the diamond tool is more wear resistant and has a longer tool life when the rake face crystal orientation is (110). Bouwelen [64] showed that as the cutting time increases, the temperature of the contact surface between the workpiece and the tool increases, and tool wear is due to the phase transition of subsurface of workpiece from the diamond (sp3) structure to the graphite (sp2) structure. Zhao [65] studied the wear of the diamond

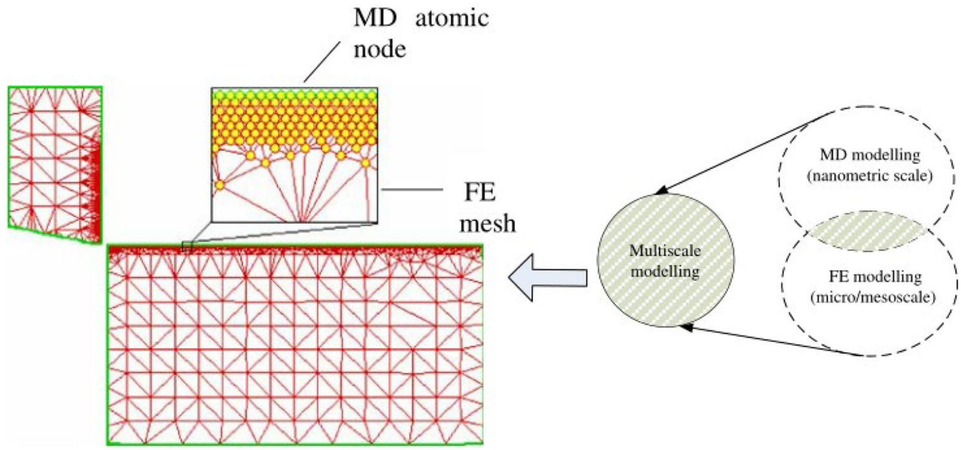

Fig. 13 Multiscale model for nanometric cutting of single-crystal aluminum [56]

tip in AFM, analyzed the friction and wear behavior of the AFM diamond tip in the process of cutting oxygen-free copper, aluminum alloy and single-crystal silicon and analyzed the surface roughness of the processed workpiece. It is found that the use of oxygen-free or low-oxygen cutting fluids during the cutting process of copper, the use of lubricants when cutting aluminum and the use of smaller feed rates and depths when cutting single-crystal silicon while ensuring low temperature and low oxygen are all effective to reduce tool wear during the cutting process [66, 67].

In the nanocutting process, according to the machining difficulty, the materials can be divided into easy-to-machine materials and difficult-to-machine materials. Common easy-to-machine materials include aluminum, copper alloy, silver and gold, and difficult-to-machine materials include silicon, silicon carbide, germanium, selenide and other materials, as shown in Fig. 16. In the process of cutting easy-to-machine materials, the tool wear is small, and the processing stroke can reach several hundred kilometers without obvious wear. In the process of cutting difficult-to-machine materials, the tool wears a lot, even when the machining stroke reaches 1 km, the tool has already experienced serious wear. At the same time, tool life is also related to tool wear. When cutting easy-to-machine materials, the service life is longer, and when cutting difficult-to-machine materials, the service life is shorter, as shown in Fig. 17 [68].

In the nanocutting process, according to the wear geometry and location, diamond wear can be divided into flank wear, notch wear, groove wear, tool tip wear and crack wear, among which flank wear and notch wear are two more serious wear phenomena, as shown in Fig. 18 [68].

By studying the nanocutting process of single-crystal copper-containing Be element, it can be found that during the cutting process, C atoms move from the diamond tool to the middle of Be atoms, but no C atoms move from the diamond tool to the middle of Cu atoms. It shows that the C element and the Be element have a chemical reaction and forms Be_2C, which intensifies the wear of the diamond tool, as shown in Fig. 19 [70, 82].

In the nanocutting process, the use of nanocutting fluid can significantly improve the wear performance of the tool

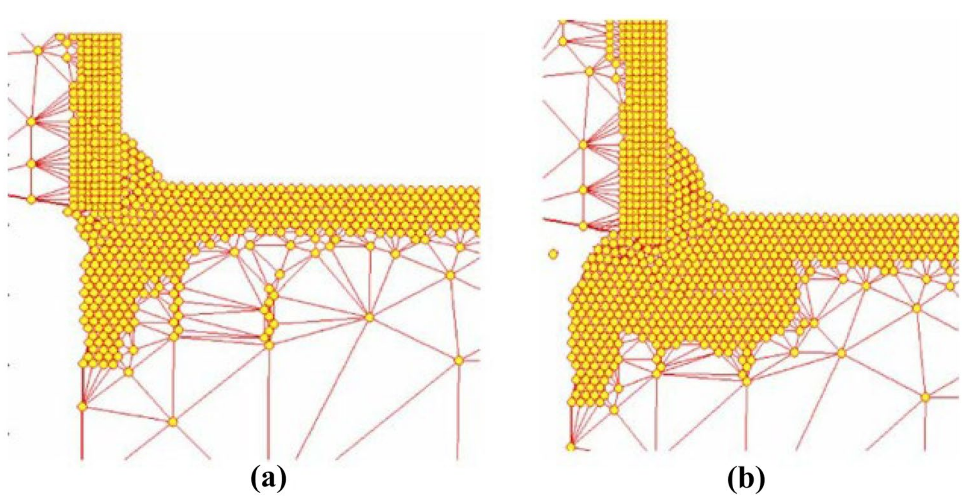

Fig. 14 The atom snapshot with motion of the tool: **a** at the 20th time step; **b** at the 43rd time step [56]

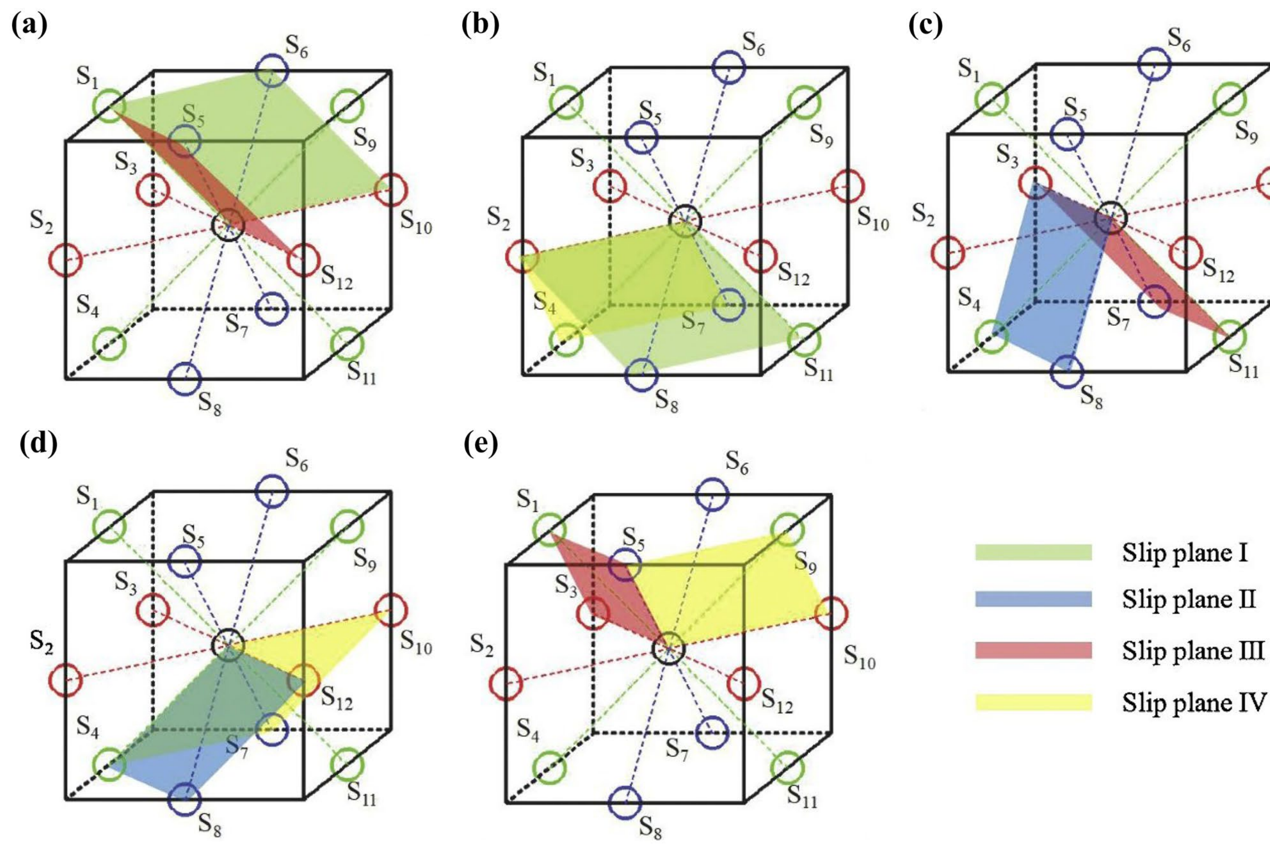

Fig. 15 The slip direction and corresponding slip planes of (**a**) S1, (**b**) S2, (**c**) S3, (**d**) S4, (**e**) S5 [62]

and provide high performance in terms of surface roughness, cutting temperature and chip morphology, as shown in Fig. 20 [71, 77, 78].

The tool wear has also strong relationship with the temperature between the tool and workpiece[76]. Cheng et al. [73] discussed the influence of temperature on the wear of

Fig. 16 Classification of easy-to-cut and difficult-to-cut materials for diamond tools in UPDM [22, 69]

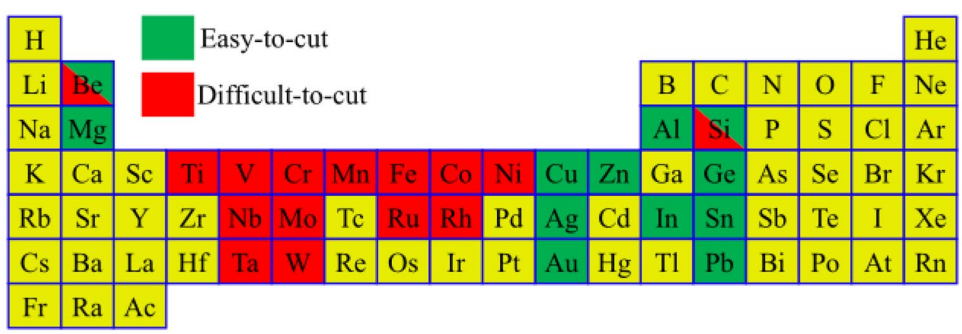

Fig. 17 Schematic map of diamond tool life for different workpiece materials [68]

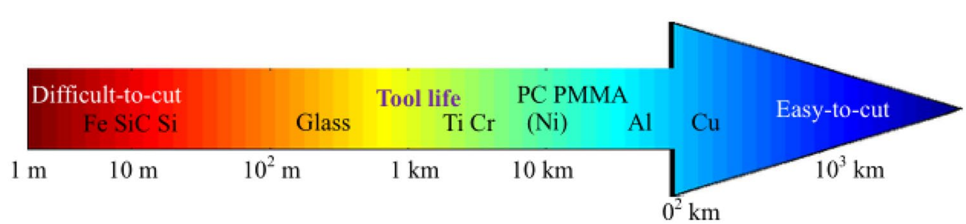

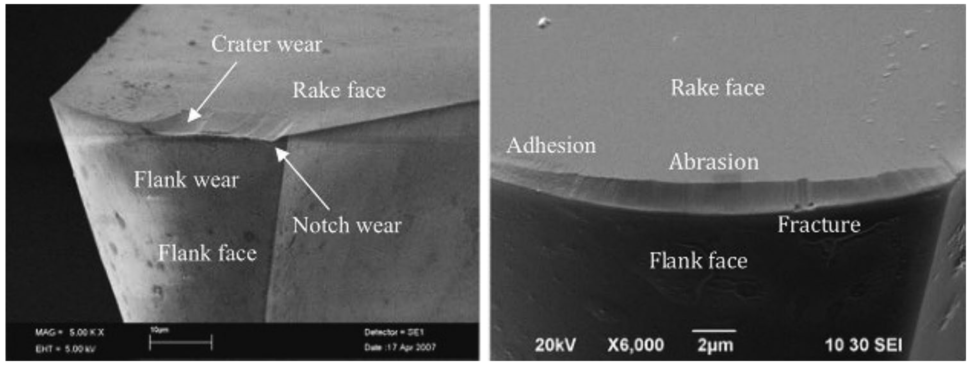

Fig. 18 SEM pictures of worn diamond tools [68]

tool in nano cutting process and verified the phenomenon by AFM cutting experiment. Through the comparison of cutting forces and tool wear condition, it was found that the basic wear mechanism of diamond tool is thermochemical wear.

The friction and wear properties of different tool materials have also been studied [80]. Kuai [79] found that the wear resistance of tool of WC-7Co is significantly better than that of WC-10Co, so the appropriate tool material is a key factor for the tool to have excellent cutting performance. The test of tool wear during nanomachining has also been carried out at different levels. Singh [81] used an interferometer to collect the cutting edge wear image of the tool and measure the profile, which provided experimental support for minimizing tool wear and optimizing machining conditions, as shown in Fig. 21.

4 Subsurface damage

Molecular dynamics simulation method is also an effective method in the study of the subsurface damage mechanism of the workpiece during the nanocutting process. Through molecular dynamics simulation of the single-crystal silicon cutting process, it can be found that during the cutting process, the subsurface has undergone a phase change of Si-I → Si-II → a-Si, and dislocations are generated at the same time, as shown in Fig. 20 [89]. The molecular dynamics simulation method can be also used to simulate the subsurface crystal morphology [90, 91]. By comparing the subsurface crystal morphology at different cutting depths, it can be found that as the cutting depth increases, the subsurface defects of the cut workpiece increase significantly. When the cutting depth is 0.7 nm, the defect thickness is about 1 nm; when the cutting depth is 1.5 nm, the defect thickness is about 2.5 nm; when the cutting depth is 2.1 nm, the defect thickness is about 4 nm. At the same time, as the cutting depth increases, the subsurface crystal structure also changes to a certain extent. When the cutting depth is less than 1.5 nm, the ratio of HCP and BCC atoms is basically stable. When the cutting depth increases to 2.1 nm, as the cutting distance increases, the ratio of HCP atoms increases, as shown in Fig. 22 [83–88]. Zhang [97] studied

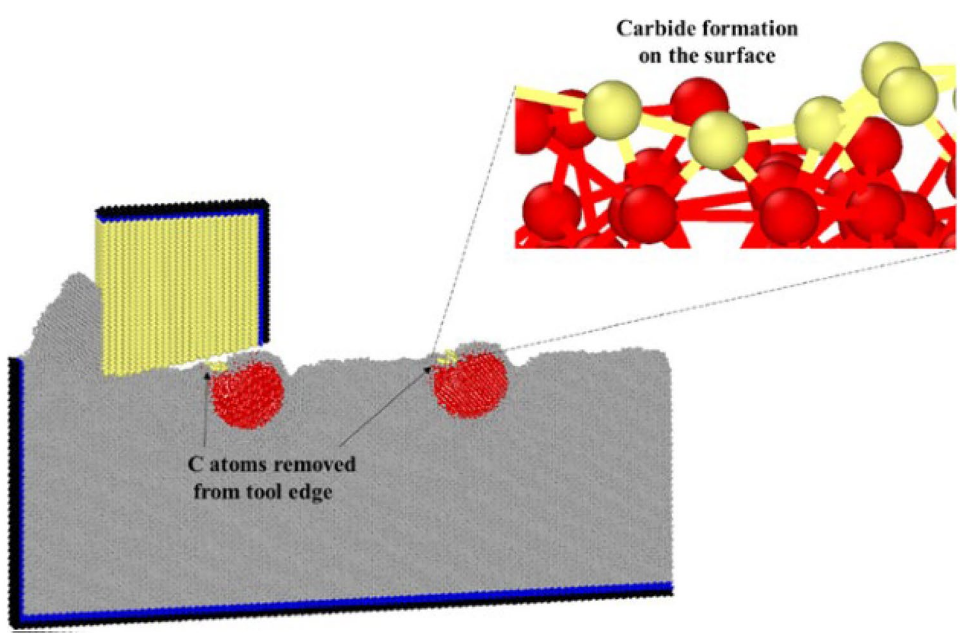

Fig. 19 Carbide formation on workpiece surface during nanocutting of CuBe [70]

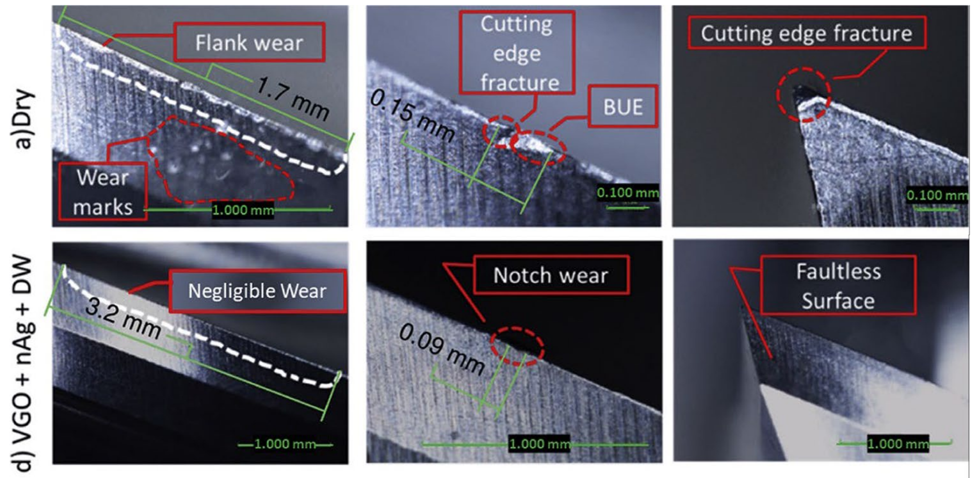

Fig. 20 Optical microscope images of tool wear examined with different zoom ratios: a) Dry, d) VGO + nAg + DW [71]

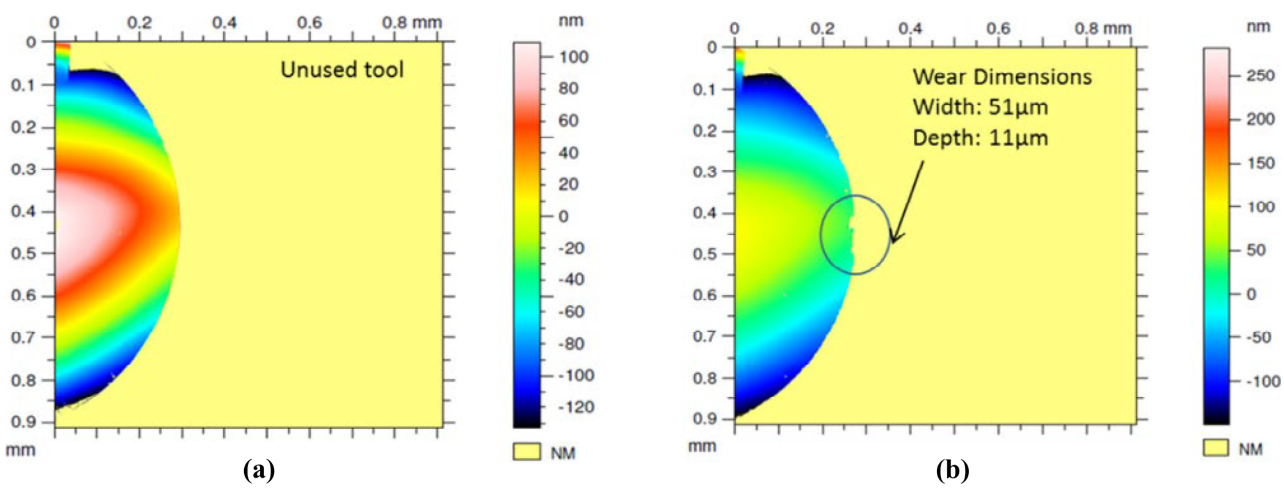

Fig. 21 (**a**) Measurement of new tool, (**b**) measurement of worn out tool after 30 cycles [81, 82]

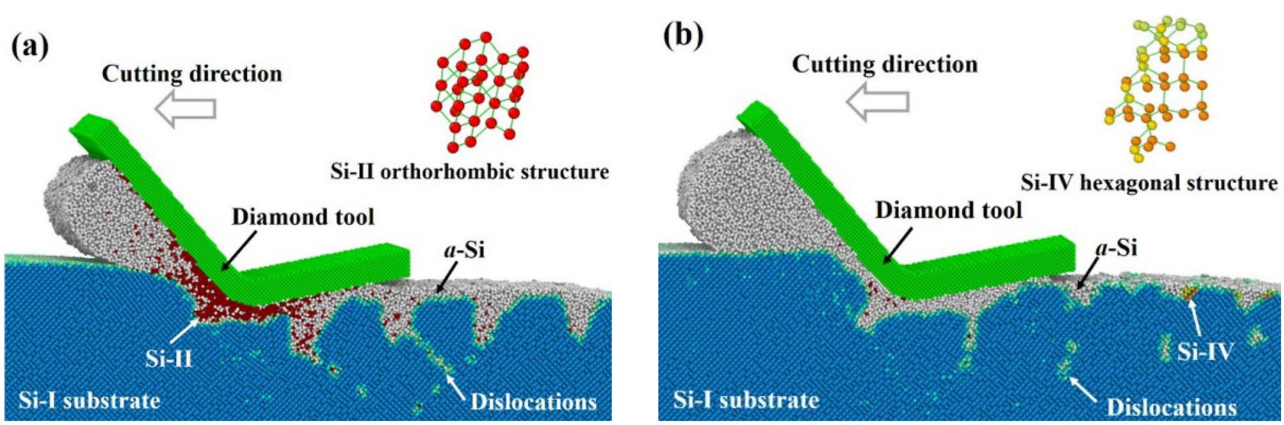

Fig. 22 MD simulation of the sc-Si nanometric cutting process. (**a**) The snapshot of the cutting process with the temperature in the contact region of 300 K; (**b**) the snapshot of the cutting process with the temperature in the contact region of 700 K. High-pressure Si-II phase is present in (**a**), and a metastable phase Si-IV is visible in (**b**) [89]

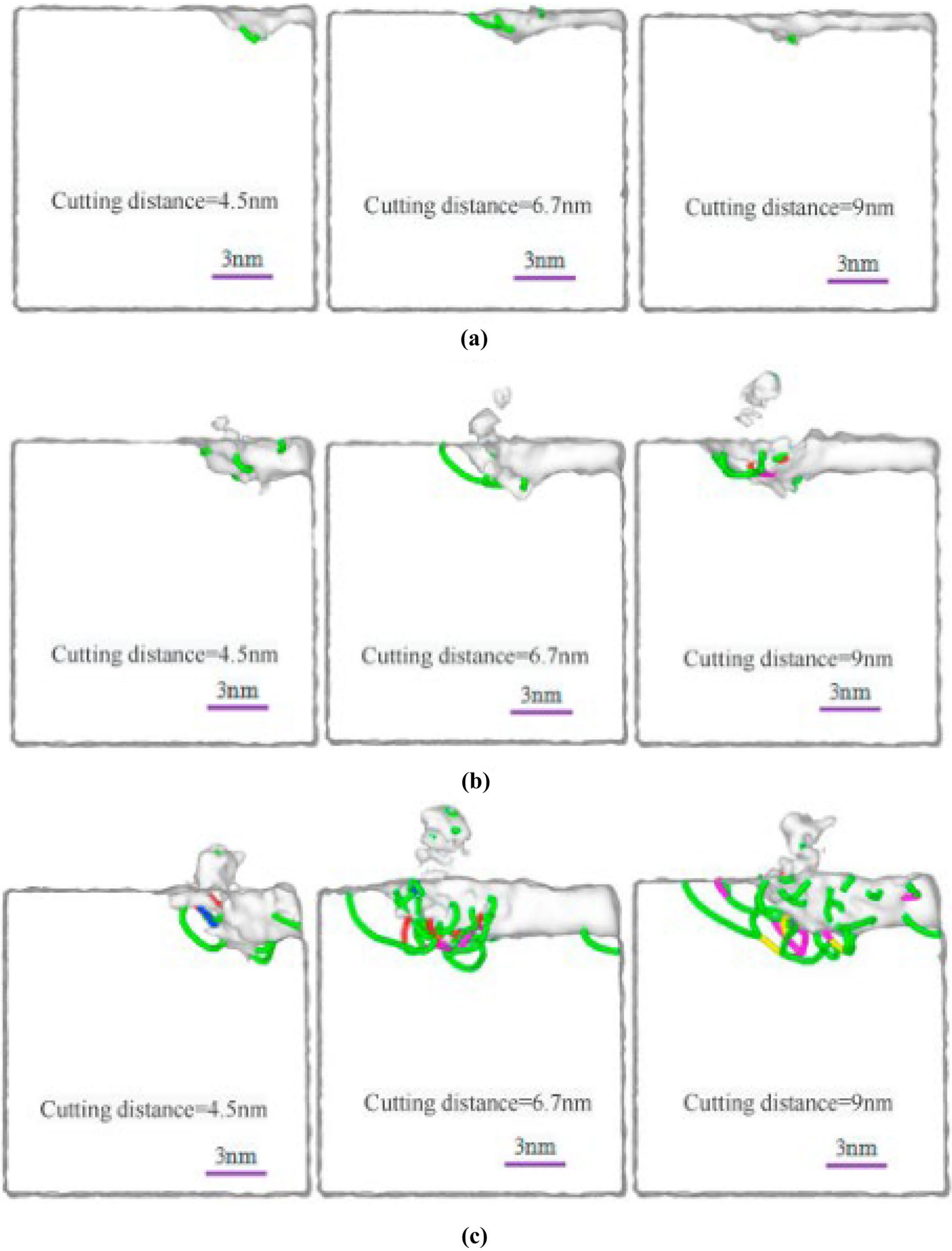

Fig. 23 Subsurface crystal structures under different cutting depths. (**a**) 0.73 nm, (**b**) 1.5 nm, (**c**) 2.1 nm [83]

the nanocutting process of single-crystal copper at different cutting speeds and cutting depths through molecular dynamics simulation and found that at the same cutting speed, the cutting depth had a significant impact on the type of crystal structure on the subsurface [98, 99].

During the nanocutting process, not only phase transition appears, but also dislocations occur at the subsurface [58, 60, 63–65]. And the types of dislocations are different under different cutting depths, as shown in Fig. 23. When the cutting depth was 0.7 nm, the type of dislocation was Shockley dislocation. With the increase in cutting depth, Shockley dislocation gradually transformed into Stair-rod dislocation, and finally, Hirth dislocation appeared [83].

By simulating the cutting process, the distribution of different crystal structure types during the cutting process can be obtained, and it can be found that the HCP crystal structure accounts for the largest proportion during the cutting process. At the same time, it can be found that dislocations continue to increase and eventually form grain boundaries in the cutting process, as shown in Fig. 24 [93, 94].

Brittle materials are easy to produce crack and damage during ultraprecision machining, which has an adverse effect on the performance of cutting materials. Therefore, it is necessary to conduct in-depth research on the crack generation mechanism of brittle materials. Chen [95] carried out molecular dynamics simulation of nanocutting process on brittle gallium arsenide, studied the crack generation mechanism of gallium arsenide under different cutting parameters and found that in the process of high-speed nanocutting, the damage in the subsurface of gallium arsenide is mainly changed from dislocation to phase transformation and amorphization, and there is a high value of tensile concentration stress, which leads to the formation of crack, as shown in Fig. 25.

To study the subsurface damage in the nanocutting process, the RDF (radial distribution function) can also be used to characterize the subsurface crystal structure changes. The RDF represents the particle density which is the function of the distance from the reference atom, and its value is the ratio of the regional density to the global density of the particles in the periodic boundary box. The regional density is the ratio of the particle number of spherical shell to the volume of the spherical shell, and the global density is the ratio of the total number of particles in the box to the volume of the box. By selecting Si–C, Si–Si/C–C, Si–C in SiC and Si–Si atom pairs in polycrystalline SiC, the RDF of SiC subsurface during nanocutting can be obtained, as shown in Fig. 26. It can be found that during the cutting process, the RDF peaks of the atom pairs are reduced, indicating that the atoms inside the subsurface crystal have migrated and the crystal structure has changed during the cutting process. And it can be found that the amorphous structure appears in

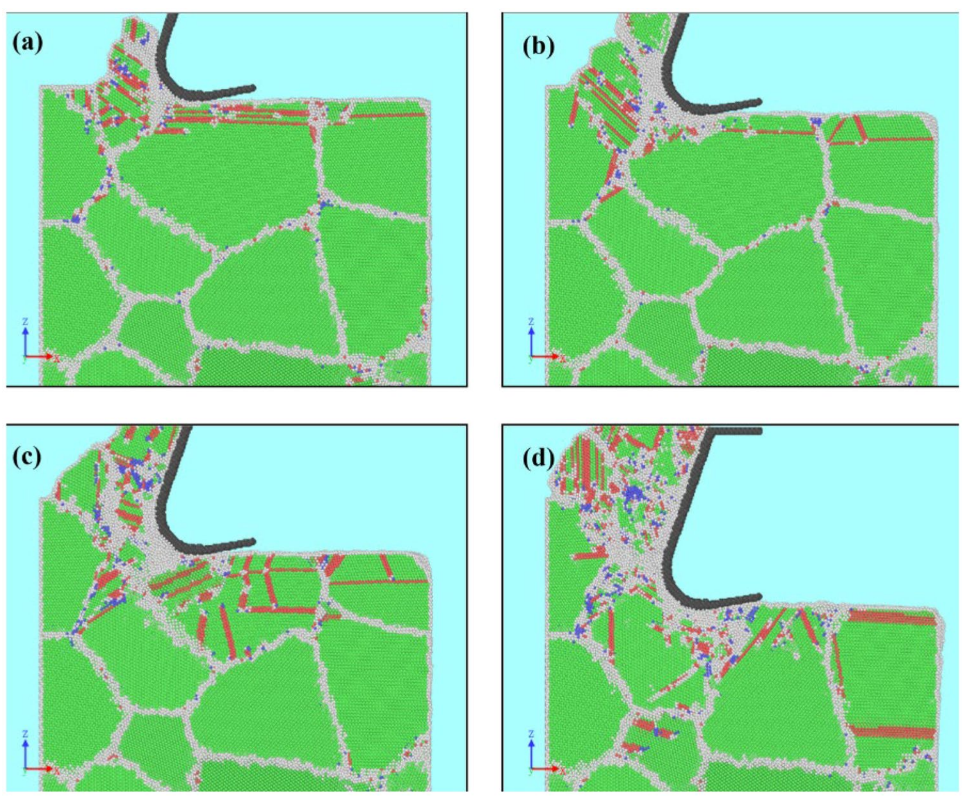

Fig. 24 CNA images of the transformation process between dislocations and grain boundaries [93]

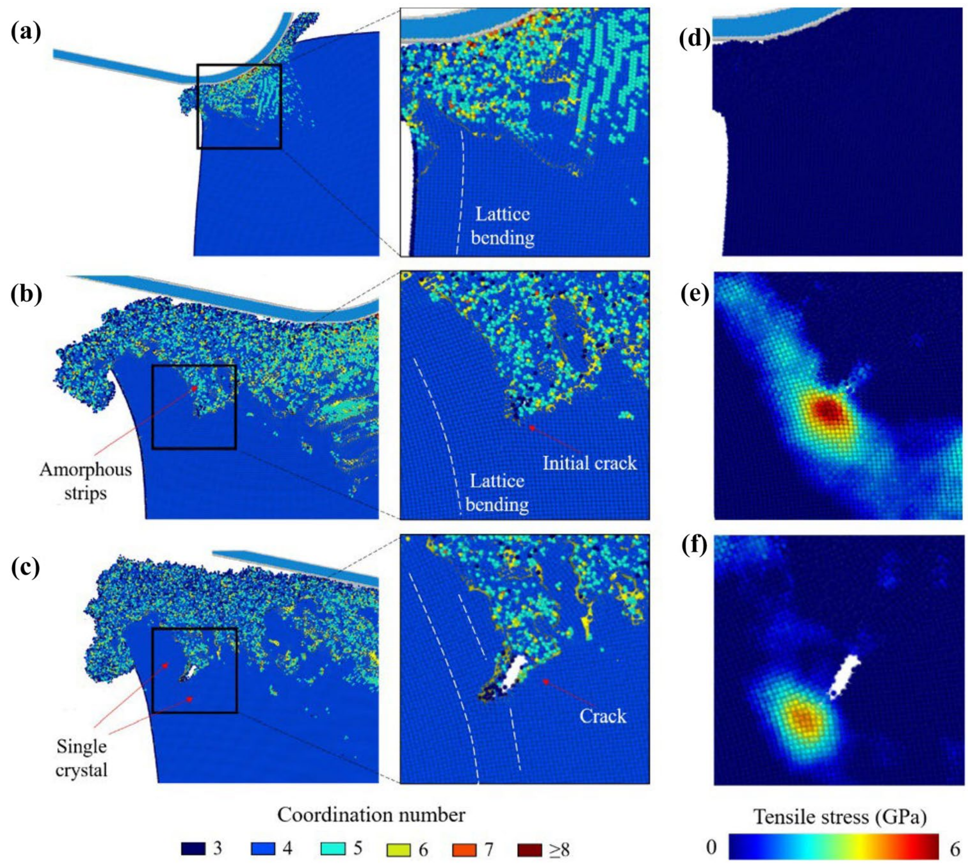

Fig. 25 The crack formation process in model with tool radius of 76 nm colored with the coordination number and tensile stress, when the cutting distance is (**a**, **d**) 30 nm, (**b**, **e**) 42 nm, (**c**, **f**) 54 nm [95]

the chip and the subsurface of the cutting surface, but there is no amorphous structure inside the workpiece, indicating that the amorphous state is formed on the cutting subsurface during the cutting process, as shown in Fig. 27 [97].

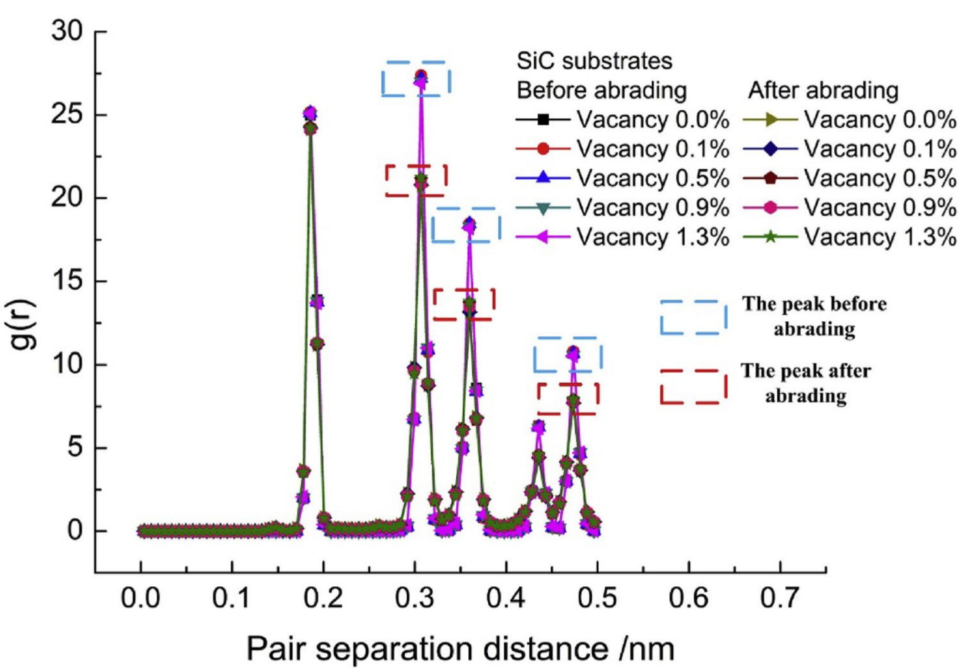

Fig. 26 RDF of SiC substrates before after nanoabrasion [97]

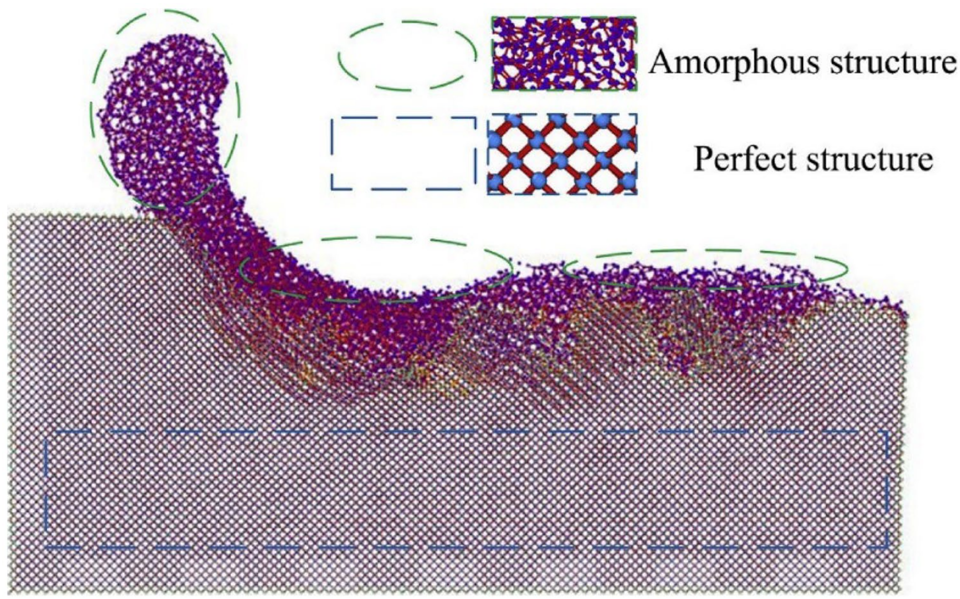

Fig. 27 The structural transformation of SiC substrates after abrasion [97]

In the research of subsurface damage mechanism in nanocutting process [100–102, 131], Raman spectroscopy is a fast non-destructive testing method used to characterize the structure of materials. Raman spectroscopy can detect the phase transition of the crystal from crystalline to amorphous during the nanocutting process, and at the same time, it can detect the residual stress during the nanocutting process. In the polycrystalline germanium cutting process, Raman spectroscopy is used to characterize the deformation and damage of the subsurface during the cutting process. When a tool with a rake angle of -30° is cutting along the (100) direction of the polycrystalline germanium surface, the Raman spectrum Ge-I bands of the machined surface with different cutting depths are shown in Fig. 28. It can be found that the Raman spectrum peak at 300 cm^{-1} decreases with the increase in the cutting depth, indicating that the crystal defects increase with the increase in the cutting depth. At the same time, it can be found that when the cutting depth is less than 131 nm, there is almost no Raman spectrum peak shift, while when the cutting depth is between 131 and 169 nm, a certain Raman spectrum peak shift will occur, indicating that the amorphous germanium is formed in the subsurface, as shown in Fig. 29 [104].

Raman spectroscopy can also be used to measure the subsurface residual stress of the workpiece during the cutting process. For example, the subsurface stress can be obtained

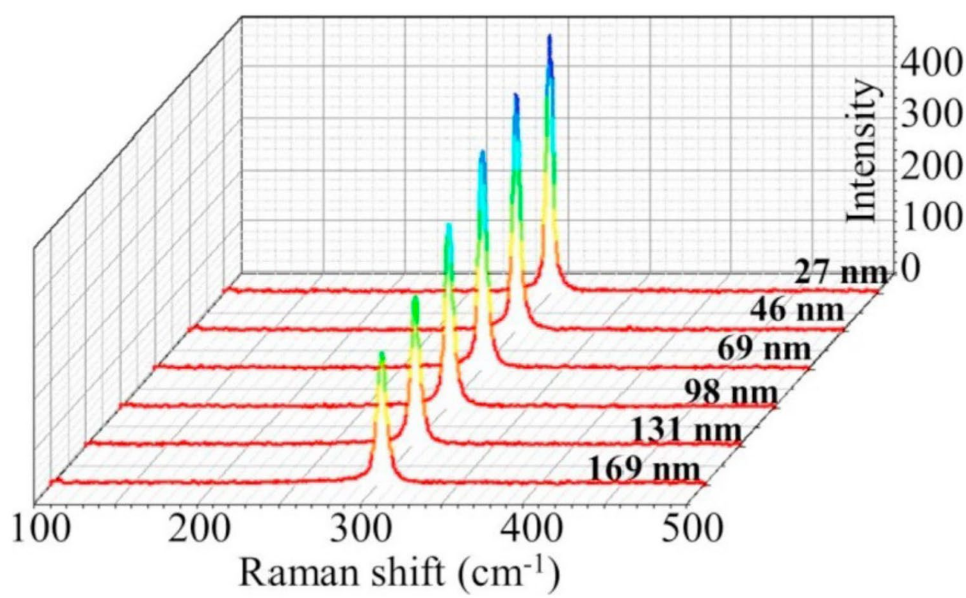

Fig. 28 Raman spectra of the machined surfaces with different UCTs after taper cutting (θ:-30°, cutting orientation: 001(100)) [104]

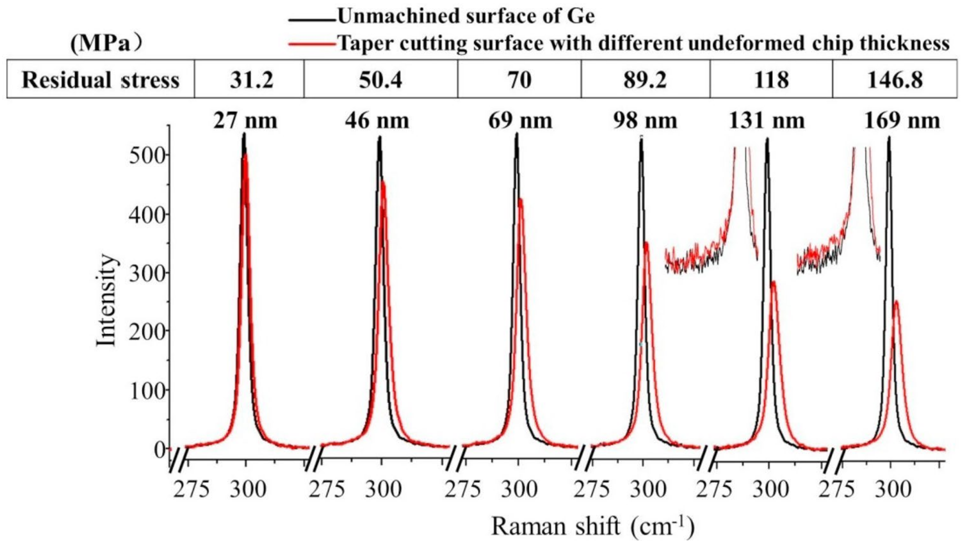

Fig. 29 Comparison between the Raman spectra of the machined and unmachined surfaces of germanium. The residual stresses calculated based on the shift in the Ge-I peak are shown above the Raman spectra (θ:-30°, cutting orientation: 001(100)) [104]

by performing Raman spectroscopy on the subsurface during the SiC cutting process, as shown in Fig. 30 [105].

To study the subsurface physical change mechanism of the workpiece, nano-FTIR spectroscopy can be used for detection and analysis. Nano-FTIR spectroscopy is a kind of infrared near-field spectroscopy based on Fourier transform, which can be used to perform spectral analysis on the surface of materials and display surface changes, as shown in Fig. 31 [106].

5 Cutting force

The cutting force in the nanocutting process is an important property to characterize the nanocutting process [103, 115, 117, 119–121]. In the nanocutting process of SiC, the lower value of the cutting force represents that the cutting mode is likely to be brittle cutting, and the higher value represents that the cutting mode is likely to be plastic cutting. So the cutting force amplitude can also be used to determine whether the cutting process is plastic cutting or brittle cutting, as shown in Fig. 32 [107–111, 122, 123]. The tools used for the cutting force detection are summarized in Table 4.

By studying the change in cutting force during the nanocutting process [124, 127, 128, 150], the cutting force in x and y directions at different cutting depths and the formation mechanism of cracks during the cutting process can be acquired, as shown in Fig. 33. The dotted and solid line in Fig. 34 represents the cutting force in x and y directions at a cutting depth of 4 nm, as shown in Fig. 33. In the process of nanocutting of lutetium oxide, when the cutting stroke is before 45 nm, the cutting force presents a tendency of increasing first and then fluctuating steadily. When the

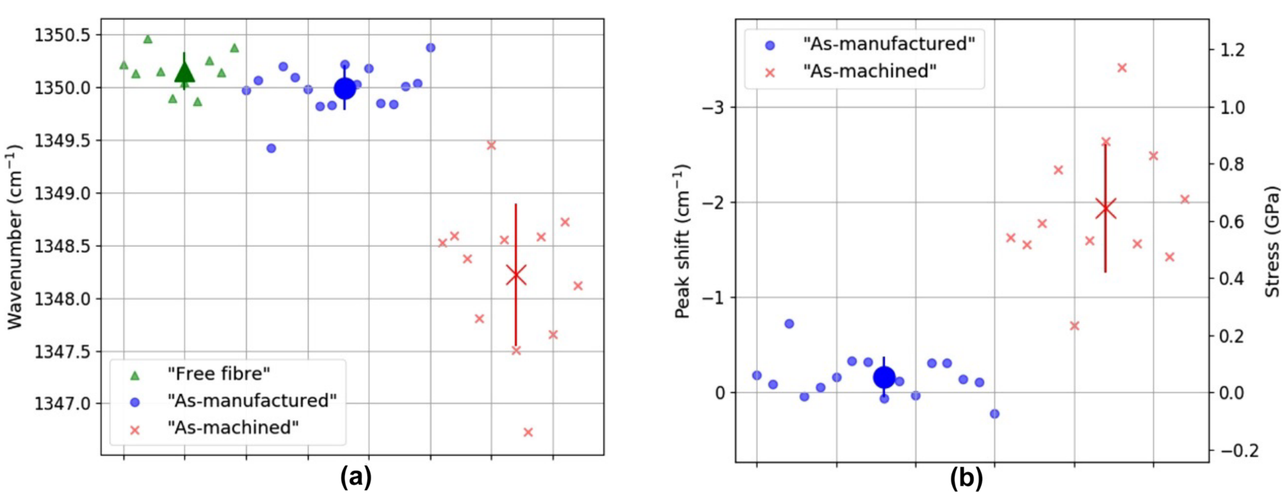

Fig. 30 Residual stress analysis [105]

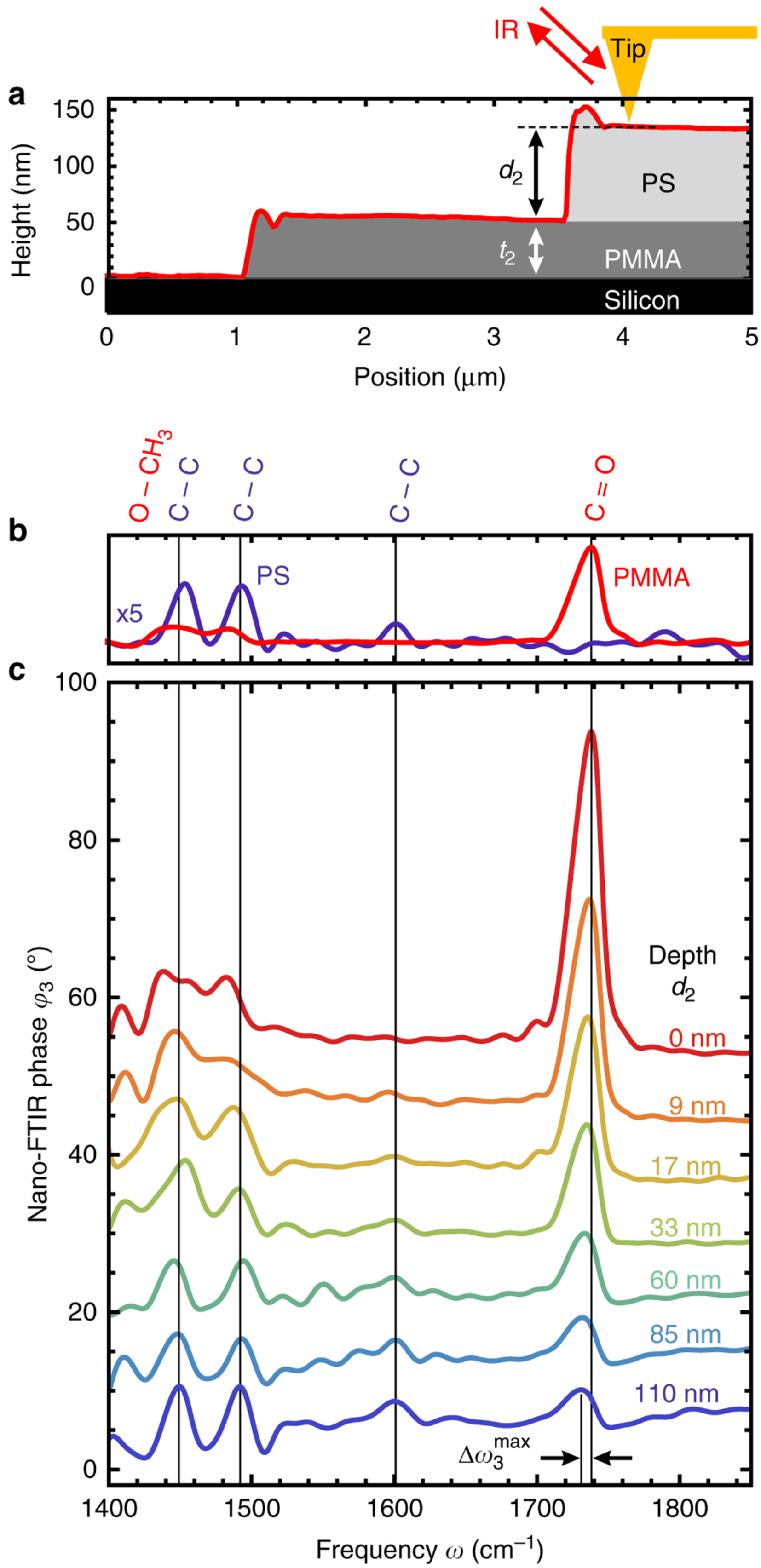

Fig. 31 Subsurface nano-FTIR spectroscopy experiments on well-defined multilayer samples. **a** Schematics of the experiment and PMMA/PS test sample, including the topography line profile of a $d_2 = 85$-nm-thick PS layer covering the $t_2 = 59.4$-nm-thick PMMA layer on Si. **b** Reference nano-FTIR phase spectra recorded on thick PMMA and PS layers. **c** Subsurface nano-FTIR phase spectra of PMMA at different depths d_2 below PS (average of 50 spectra (80 spectra for $d_2 \geq 85$ nm), 30-s acquisition time per interferogram, ×128 zero filling, 17 cm^{-1} spectral resolution). Black arrows in c indicate the spectral peak shift [106]

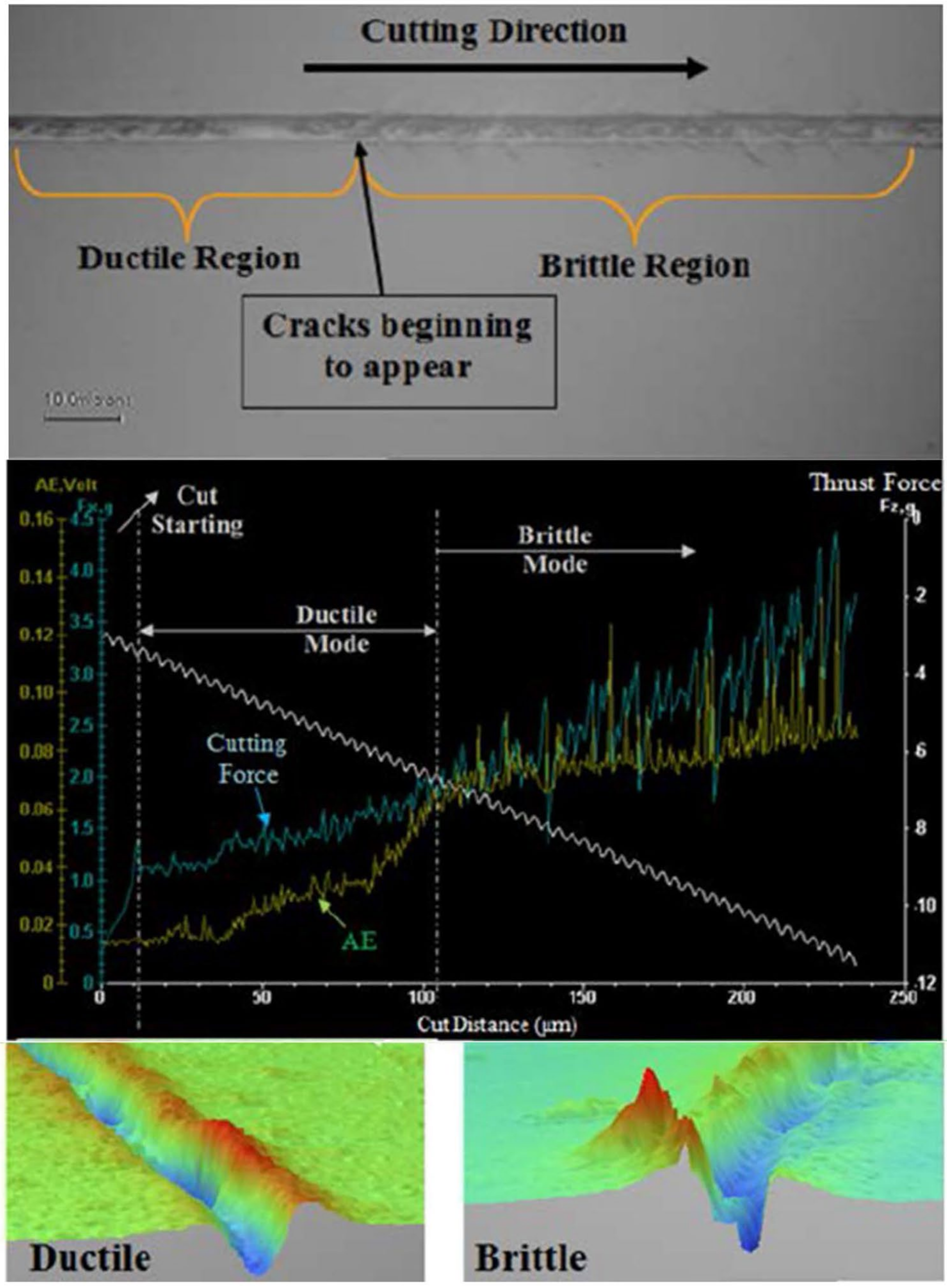

Fig. 32 Cutting force and acoustic emission data to distinguish brittle-regime with ductile-regime machining [107]

cutting stroke is at 47 nm-50 nm, the cutting force begins to drop sharply, and at this time, it can also be found that there is a crack inside the workpiece. Therefore, the change in cutting force can also show the existence of internal cracks in the workpiece during the cutting process [113].

In the nanocutting process, cutting force measurement has always been an important issue. By establishing the relationship between the cutting force, the normal force and the material removal rate, a model for predicting the cutting force during the nanoscratch process was obtained. Finally, it is found that the predicted results are in good agreement with the experimental results, as shown in Fig. 35 [116].

In the ultraprecision cutting process, due to workpiece installation errors, the cutting surface of the workpiece will be tilted, which requires a lot of time to adjust the workpiece and the tool. In another case, because the processed surface is a curved surface, it is necessary to know the curved surface information in advance before designing the processing path, and the design process is complicated. In order to solve the above problems, an adaptive processing method was proposed, which can automatically design the processing path according to the shape of the processed surface, therefore achieving high-efficiency ultraprecision processing. The adaptive processing method can adopt the combination of

Table 4 Tools used in measurement of cutting force by molecular dynamics and experiments

Authors	Methods	Tools	Results
Goel et al. [112]	Experiment	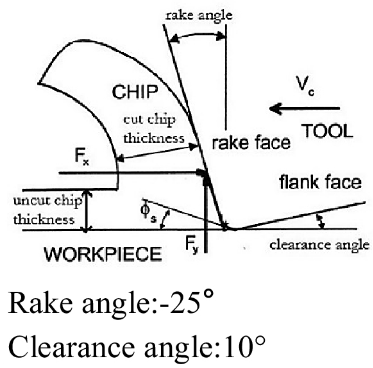	Cutting forces, Cutting morphology
He et al. [113]	MD	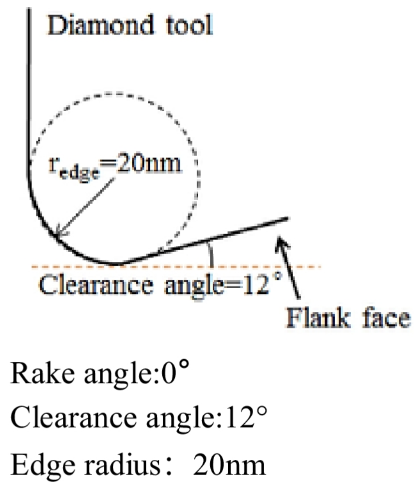	Cutting forces
Li et al. [114]	Experiment	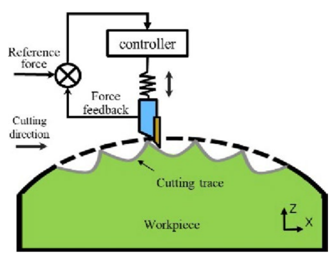	Cutting forces, Cutting morphology
Kong et al. [116]	Experiment	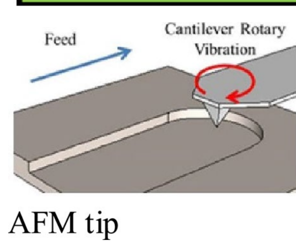	Material removal rate, cutting forces
Kong et al. [118]	Experiment	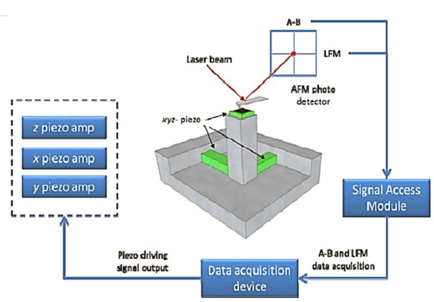	Machining force

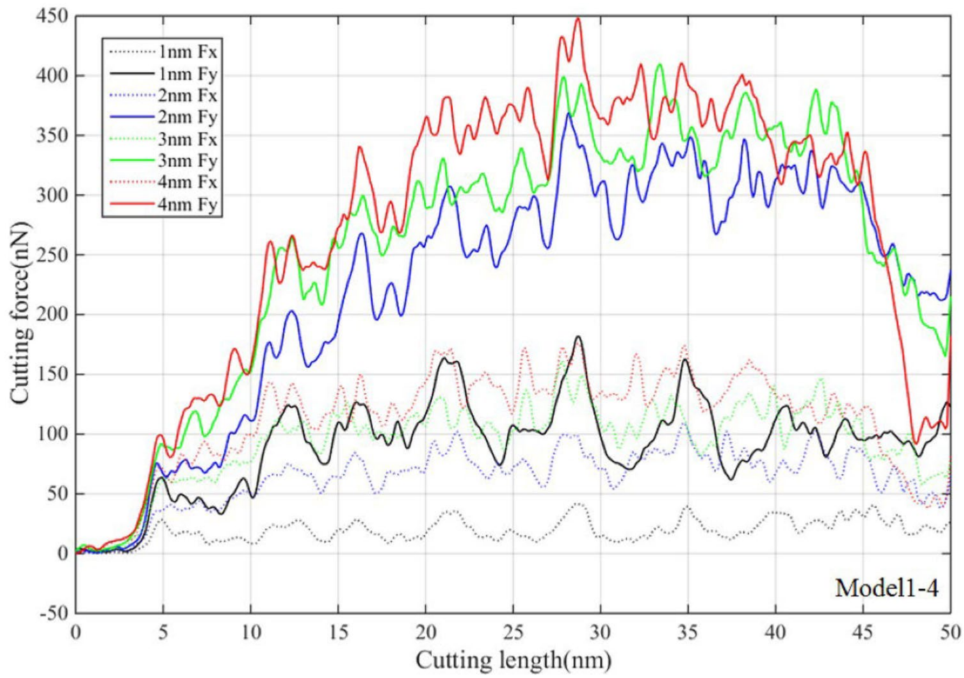

Fig. 33 Curve of cutting force in different models (cutting speed = 500 m/s): Models 1–4 refer to cutting depth 1 nm, 2 nm, 3 nm and 4 nm, respectively [113]

AFM and ultraprecision machine tools to achieve constant cutting force during processing, but this method has the disadvantage of low processing accuracy. By adopting a cutting force control system based on a flexible drive mechanism, high-precision adaptive machining can be realized. By controlling the expected loading force, a relatively stable cutting depth can be obtained. It can be found that when the applied loading force is 12mN, 18mN, 24mN, 30mN, 45mN, 60mN and 90 mN, the average cutting depth is 59 nm, 83 nm, 112 nm, 139.7 nm, 179.2 nm, 228.6 nm and 309.5 nm, respectively, as shown in Fig. 36. The shape of the processed curved surface is shown in Fig. 37 [114].

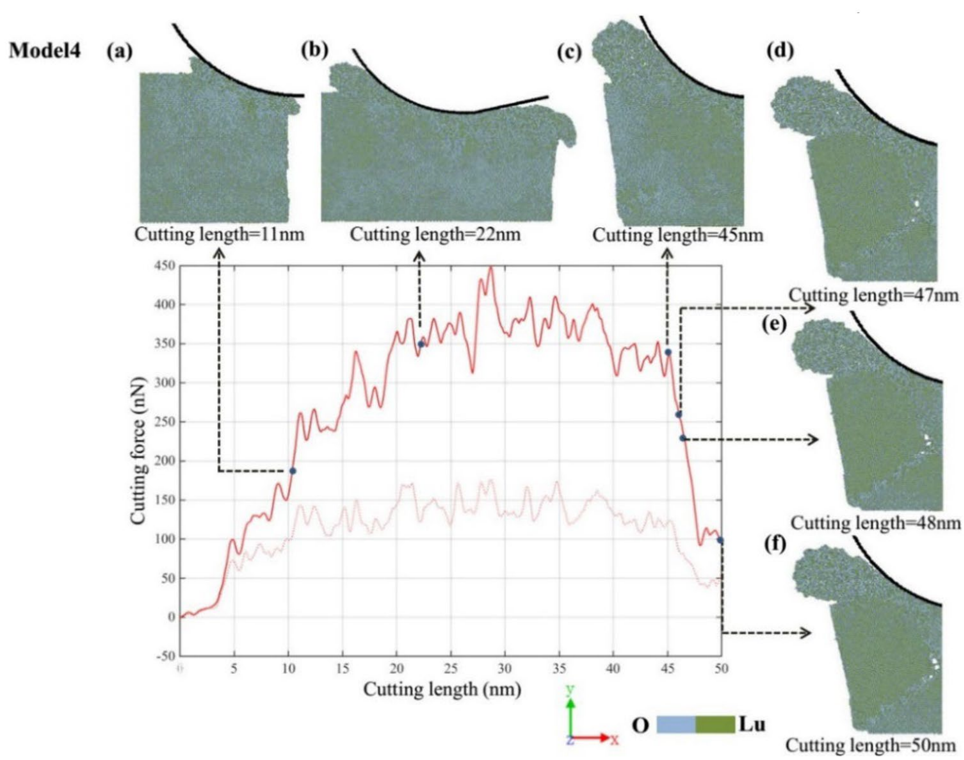

Fig. 34 Crack formation process in Model 4 (cutting speed = 500 m/s, cutting depth = 4 nm): (**a**) Before steady stage. (**b**) Steady stage. (**c**) Before crack initiation. (**d**) Crack initiation. (**e**) Crack extends. (**f**) Further extension [113]

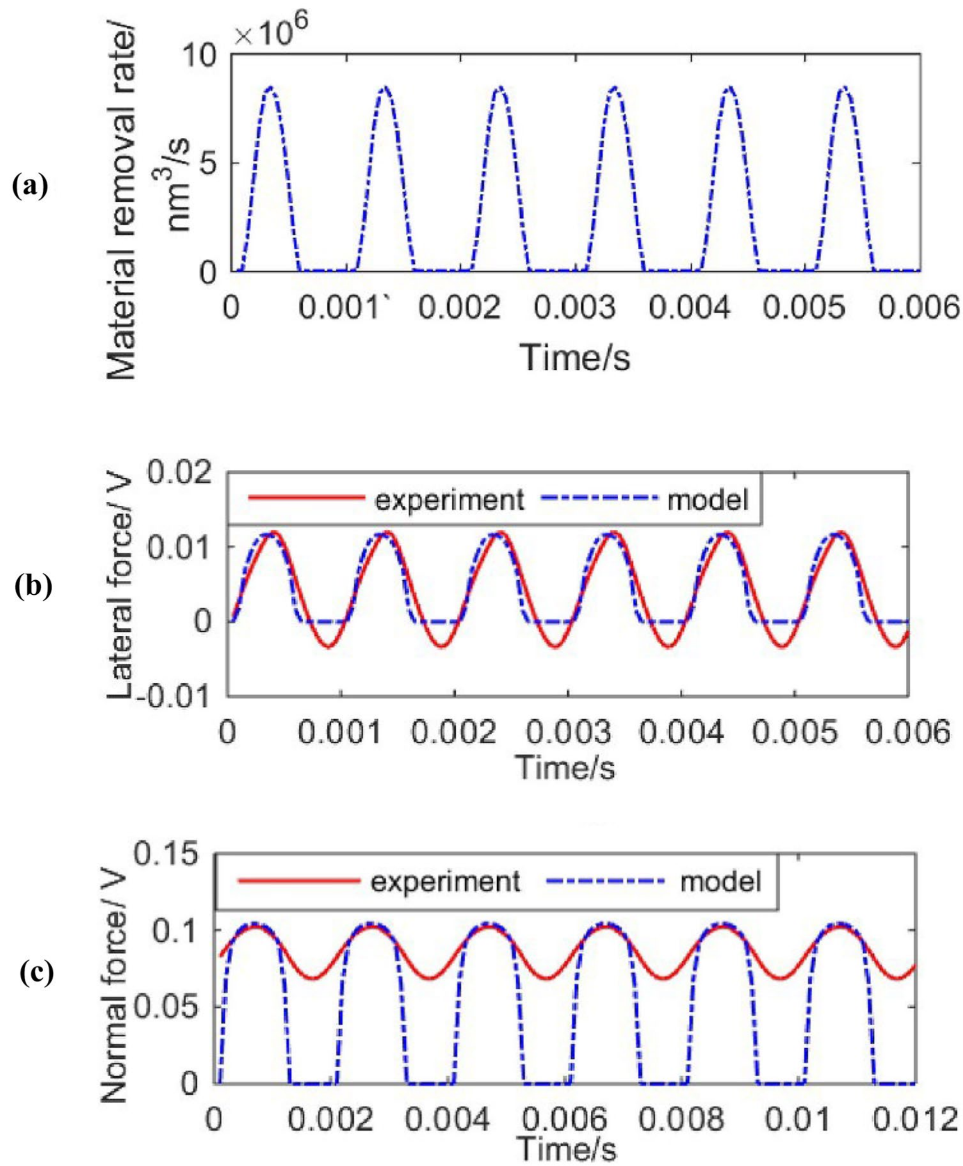

Fig. 35 (**a**) Calculated material removal rate during machining cycles. (**b**) Predicted and measured lateral force. (**c**) Predicted and measured normal force [116]

6 Friction and friction coefficient

When the diamond tool is cutting the surface of the workpiece, a certain amount of friction and wear will occur between the tool and the workpiece. When the friction and wear reach a certain level, the machining accuracy of the tool is reduced, and the tool needs to be replaced for the next cutting. Therefore, it is a very necessary problem to study the friction phenomenon and mechanism in the cutting process. The coefficient of friction during the cutting process can be obtained by calculating the ratio of the cutting force to the loading force during the cutting process, as shown in Figs. 38 and 39 [34, 125, 126, 129, 130, 133–135].

The material machinability can also be judged by the friction force and the friction coefficient. Islam [84] found that the friction coefficient was large when the material was removed by grinding, while the friction coefficient was small when it was removed by cutting, which shows that efficient removal of material can be more easily achieved by cutting, as shown in Fig. 40. At the same time, it can also be found that as the cutting depth increases, the friction coefficient also increases. Finally, it was found that the friction coefficients of different materials were not the same. For example, the friction coefficient of Cu is about 0.5, but it is about 0.4 for Ni.

The accurate determination of the friction coefficient during nanoscratch is a valuable research problem in the field of nanofriction [134, 136]. Carreon [132] simulated the actual working condition of the nanoindenter by considering the spherical shape, used the established analytical formula for the analysis of friction coefficient, then compared with the

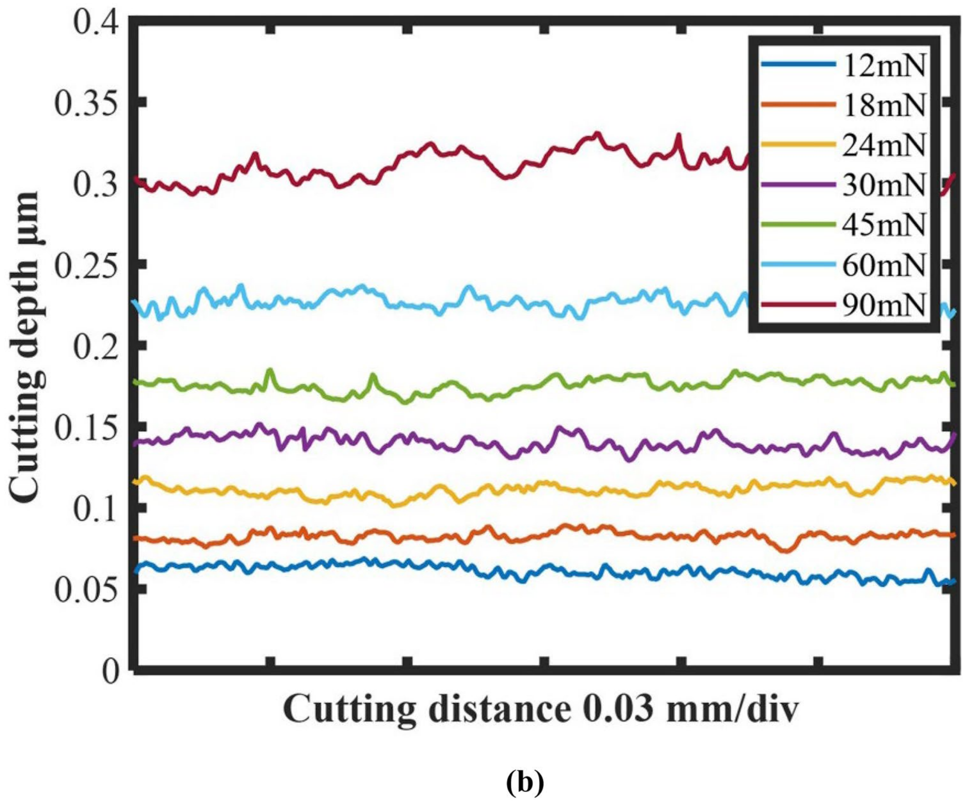

Fig. 36 (**b**) The cutting depths at different reference forces for the copper [114]

experiment results and found that the description of the friction coefficient is more accurate by considering the spherical shape of the nanoindenter, as shown in Fig. 41 [137].

7 Nanocutting experiment

Nanocutting experiments can be implemented in ultraprecision machine tools and nanoscratch instrument. In the nanoscratch test, a nanoscratch tester is used for the scratch test, as shown in Fig. 42 [138, 142–145, 148, 149]. The facilities used in the nanocutting experiments are shown in Table 5.

By conducting nanoscratch experiments on copper alloys, it is possible to obtain the nanoscratch morphology of copper alloys under different phases, as well as the relationship between the scratch depth and the scratch displacement, as shown in Table 6 and Fig. 43 [151]. Among them, the maximum loading force is 10uN, 20uN, 30uN and 40uN, respectively.

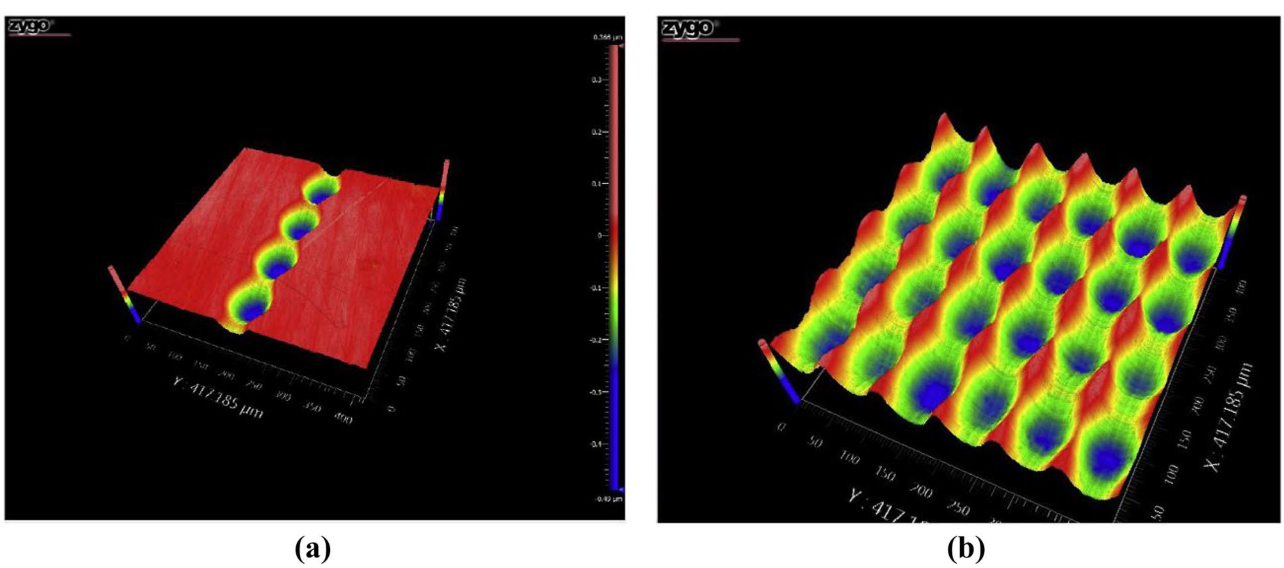

Fig. 37 The three-dimensional fabrication of the (**a**) sine-shaped microstructure and (**b**) microstructure array on copper surface [114]

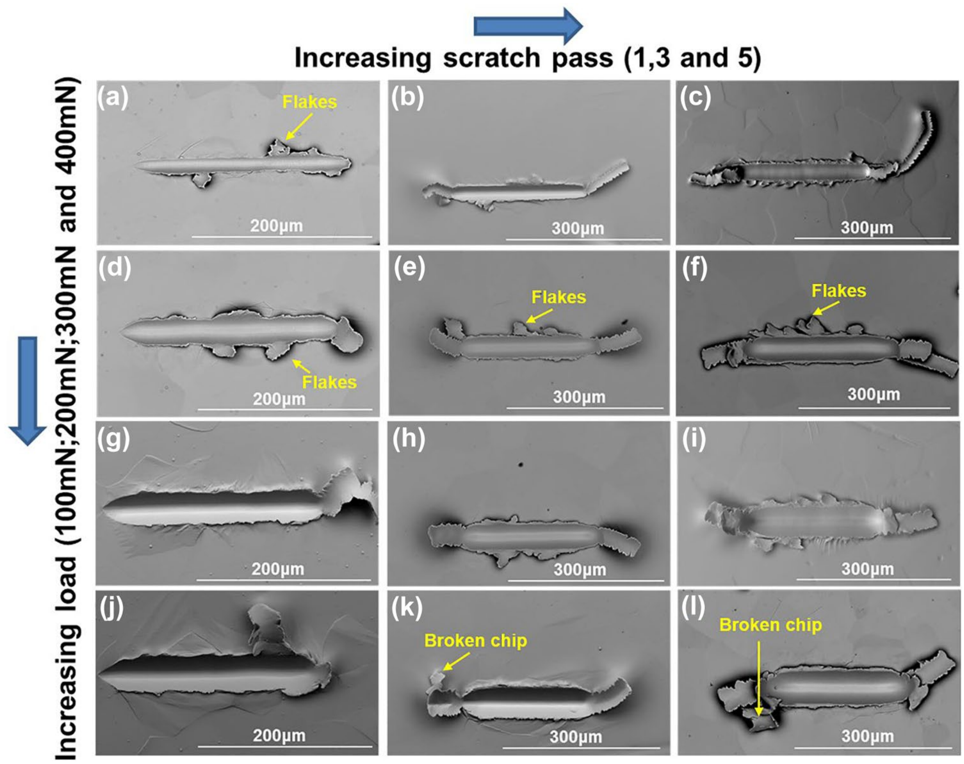

Fig. 38 SEM micrographs showing scratch wear track for different loads and scratch passes [125]

Nanocutting can be used to realize the manufacture of nanostructures. By using the AFM diamond probe to scratch on the surface of the silicon-based workpiece and apply a certain vertical load while scratching, the manufacture of nanodots, linear nanostructures, nanobosses and nanocharacters can be realized [116, 140], as shown in Figs. 44 and 45. This nanocutting method does not need to apply voltage to the AFM probe, so it is a very promising nanofabrication method suitable for the manufacturing

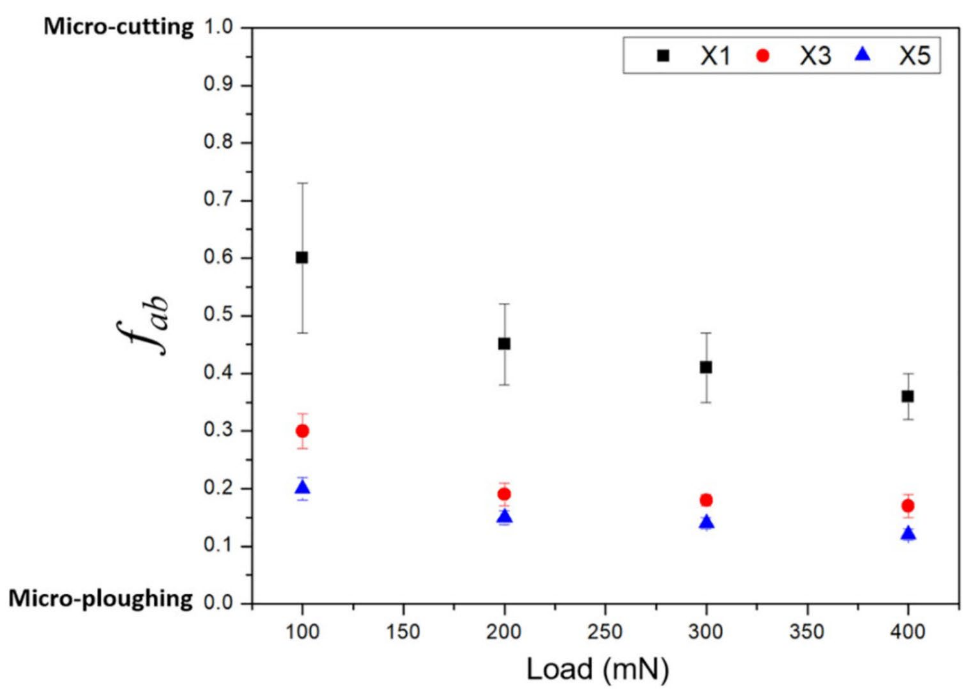

Fig. 39 Effect of the load and the number of passes on the material removal parameter (fab) [125]

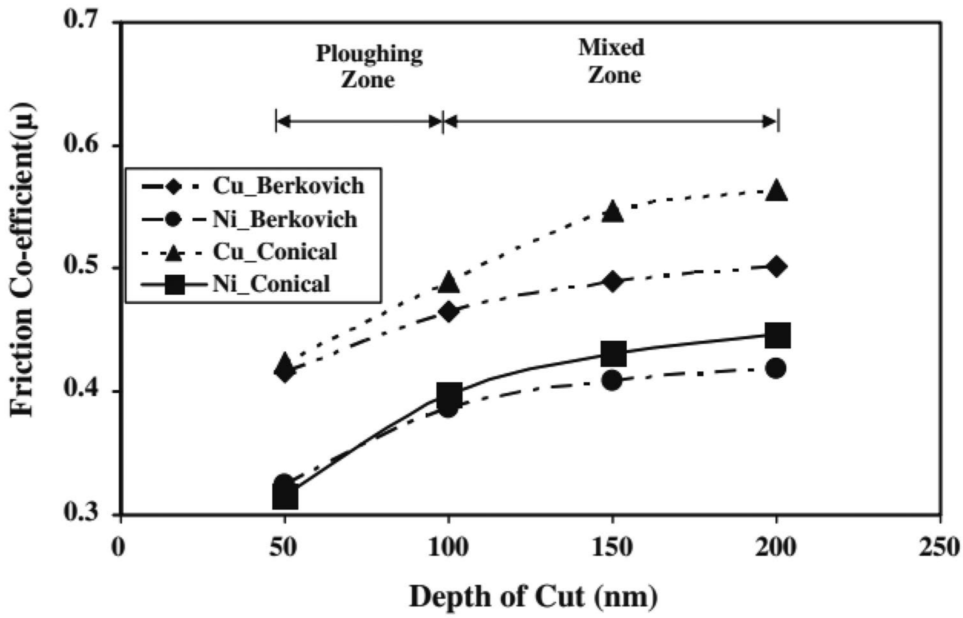

Fig. 40 The friction coefficient with respect to the depth of cut for different tool geometries and different materials [128]

process of electrical insulators such as quartz and glass in future.

Through the nanoscratch experiment, the material removal mechanism can be studied when the cutting depth is more than ten nanometers. By selecting GaAs as the nanoscratch experiment object, and selecting the loading force of 27μN, 30μN and 33μN for the scratch test, the scratch depths of 9.2 nm, 11 nm and 17 nm were obtained. It is found that when the depth of the scratch is less than 11 nm, the material is removed by extrusion, and when the depth of the scratch is greater than 11 nm, the material is removed by cutting. Therefore, when the cutting mechanism is extrusion, only burrs are formed in the cutting process, and when the cutting mechanism is cutting, chips are formed, as shown in Figs. 46 and 47 [141, 151–159].

At the same time, in the GaAs nanoscratch experiment, the subsurface properties can be studied. As one of the direct machining methods, the machining method based on the AFM tip inevitably leads to the subsurface damage of the sample due to the contact between the tip and the workpiece,

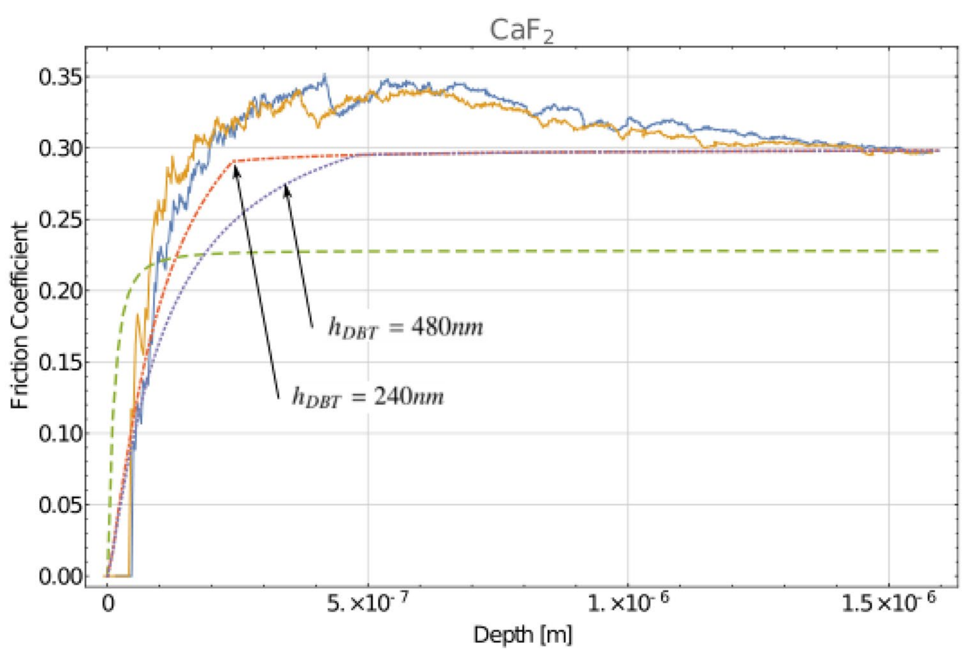

Fig. 41 Plowing friction coefficient curve of CaF2 using PAVER model. Experiments (solid orange and blue), Lafaye et al. model ($\omega = 0$, dashed green), PAVER model ($f_A = 1.067$; 240 nm) (red dot dashed), PAVER model ($f_A = 0.996$; 480 nm) (purple dotted). (For interpretation of the references to color in this figure legend, the reader is referred to the Web version of this article.) [132]

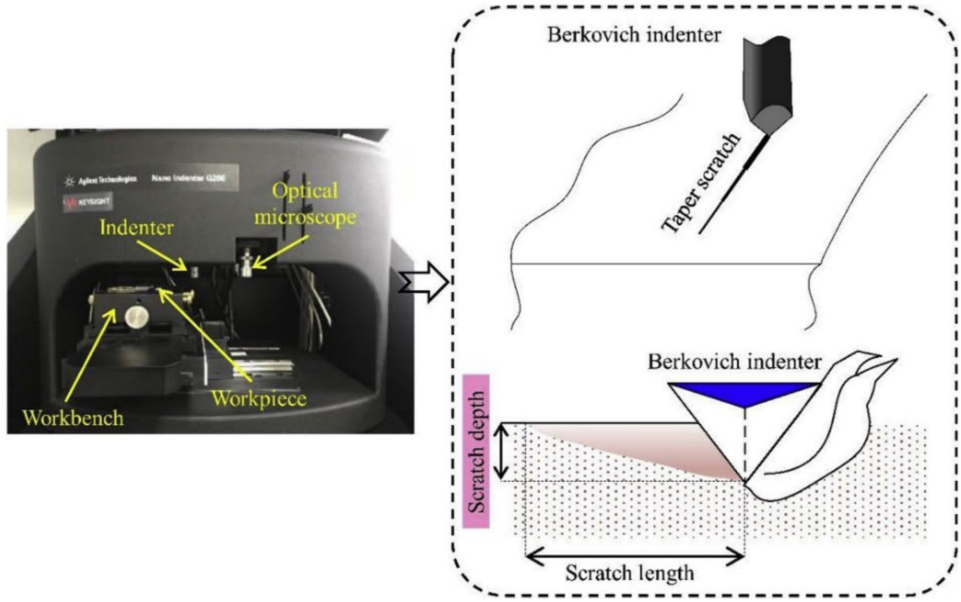

Fig. 42 Experimental setup and taper scratch schematic diagram [138]

and the subsurface defects have a decisive influence on the performance of GaAs-based devices [160]. Therefore, good subsurface quality is very important for the application of GaAs-based devices. However, the subsurface damage mechanism of GaAs in the nanoscratch process has not been fully understood. Observation of the GaAs subsurface after nanoscratch by transmission electron microscope (TEM) shows that defects, dislocations and amorphous structures are generated on the GaAs subsurface during the scratching process, which causes the damage of the subsurface, as shown in Fig. 48 [141].

In the nanocutting experiment research, the ultraprecision lathe (Moore Nanotech 350) can be used to carry out the nanometric taper cutting experiment. In the taper cutting experiment of the ultraprecision lathe, the cutting depth was gradually increased from 0 to 100 nm, and the taper was kept at 0.02°. In the experiment, taper cutting experiments with cutting depths of 10 nm and 24 nm were carried out, and the subsurface crystal morphology during the cutting process was obtained, as shown in Fig. 49. It can be found that as the cutting depth increases, the thickness of the subsurface amorphous layer decreases from 5-8 nm to 3-5 nm. And when the cutting depth is 10 nm, there is no crystal deformation under the amorphous layer. Finally, cracks were also found on the cutting subsurface, which also reflects the brittle nature of SiC [161, 162].

In the nanoscratch experiment, Raman spectroscopy can be used to test the subsurface damage mechanism during the scratching process and to characterize the phase transition process. In the unstressed state, the peak of the Raman spectrum of the workpiece subsurface reaches nearly 10,000, but it decreases slightly during plastic cutting, and the peak is 9188, indicating that the workpiece subsurface has a certain elastic deformation during the plastic cutting process, but it does not produce amorphous structure and there is no phase change. During the brittle–plastic transition cutting process, the peak value dropped sharply to about 1000, indicating that the subsurface of the workpiece had an amorphous structure during the brittle–plastic transition cutting process. In brittle cutting, the peak value is only about 150, indicating that a large amount of amorphous structure is produced on the subsurface of the workpiece during brittle cutting, as shown in Fig. 50 [163, 174].

8 Challenges and prospects

The research of nanocutting is carried out from two aspects, namely ultraprecision machine tool processing and nanoprobe processing [164–166, 185–187, 190–192]. The use of AFM probes for nanocutting is also a very effective nanoscale processing method [46, 170]. The use of AFM probes for processing has the characteristics of low cost, flexible control and high precision, as shown in Fig. 51. The fabrication of micro–nanotrenches and 3D micro–nanostructures can be achieved by AFM probes. At the same time, by integrating chemical, thermal, electrical and magnetic effects in the tip of the AFM probe, the AFM processing efficiency can be further increased [171, 173–182, 184, 188, 189, 193, 194, 200].

The traditional AFM scratching process has the problems of low processing efficiency and low material removal rate. Wang [167] proposed a nanomilling method based on AFM tip to improve processing efficiency and material removal

Table 5 Facilities used in the validation of nanocutting experiments

Authors	Methods	Facilities	Results
Yang et al. [138]	Experiment	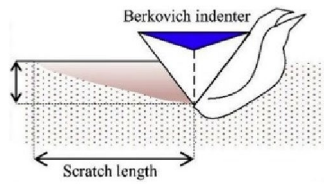 Nano indenter	Cutting forces, cutting morphology
Elkaseer et al. [139]	Experiment	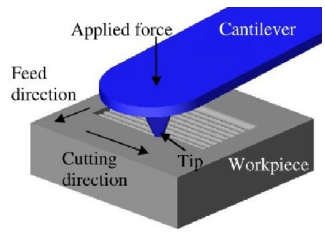 AFM probe	Cutting forces, cutting morphology, cutting depth
Yu et al. [140]	Experiment	AFM probe	Cutting morphology, cutting depth
Wang et al. [141]	Experiment	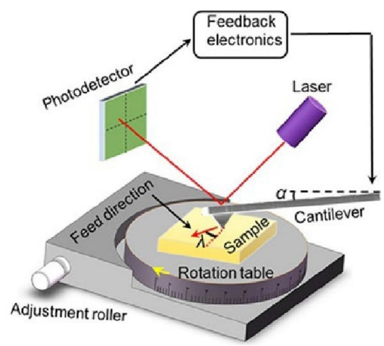 AFM tip	Cutting morphology, cutting depth, subsurface defects
Wang et al. [141]	Experiment	Ultraprecision lathe	Cutting morphology, subsurface phase change
Liu et al. [146]	Experiment	Moore 350	Cutting morphology
Gozen et al. [147]	Experiment	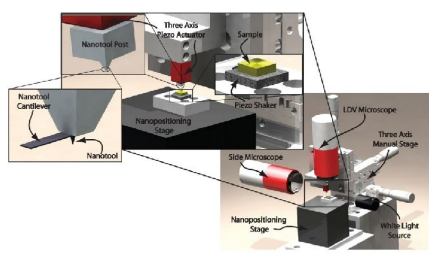 Nanomilling system	Cutting morphology

rate and conduct nano-channel processing on single-crystal silicon to study its processing mechanism. The wear rate of ultra nanocrystalline diamond (UNCD) atomic force microscope (AFM) tips in AFM applications is significantly lower than that of silicon and silicon nitride tips, so they have great potential for effective use in tip-based nanomanufacturing processes, as shown in Fig. 52 [168, 183, 195].

Recently, a new type of field emission scanning probe lithography system (FE-SPL) has been developed, which uses probes that can perform field emission. There is a certain voltage between the tip of the system and the substrate. Due to the localized effect of the tip of the electric field, when the tip of the tip is close enough to the substrate, only a very low voltage can be applied to achieve

Table 6 Profiles obtained along the length of each groove [139]

	α phase	β phase
Groove 1 [0-10] μN	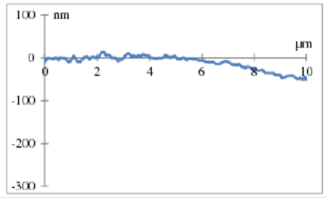	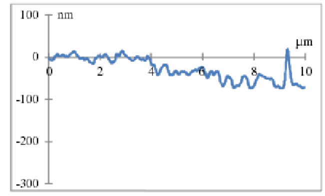
Groove 2 [0-20] μN	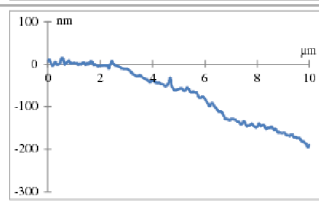	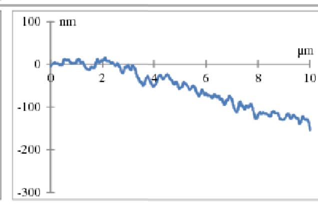
Groove 3 [0-30] μN	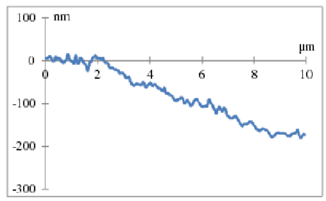	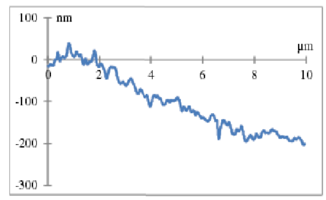
Groove 4 [0-40] μN	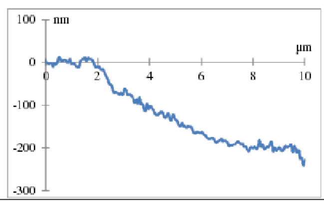	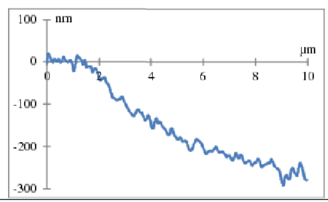

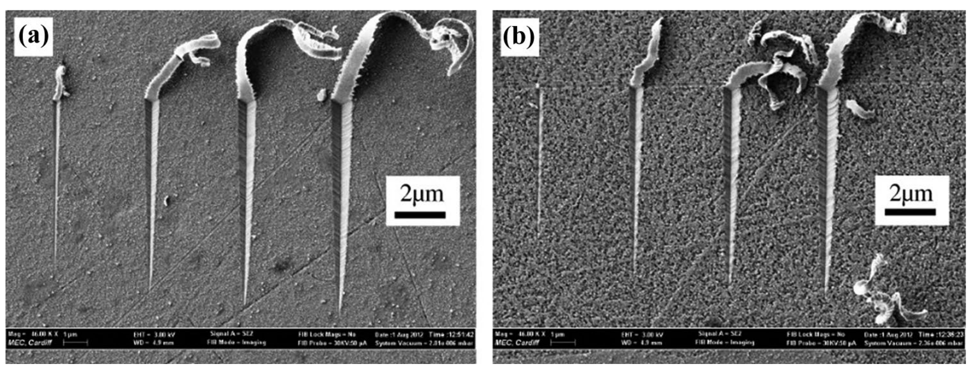

Fig. 43 Scratch tests conducted to determine the minimum chip thickness and the elastic recovery of the (**a**) α phase and (**b**) β phase [139]

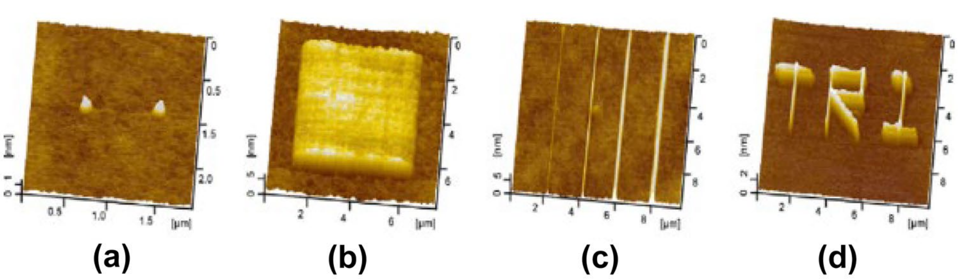

Fig. 44 (**a**) Friction-induced nanodots on Si(100) by line scratch with D = 10 nm, N = 100 and Fn = 10 μN; (**b**) surface isolated mesa by scanning scratch with N = 15 and Fn = 85 μN; (**c**) nanoline array by line scratch with N = 100 and Fn = 45, 55, 85 and 135 μN, respectively; (**d**) nanowords of "TRI" by line scratch with N = 50 and Fn = 50 μN [30]

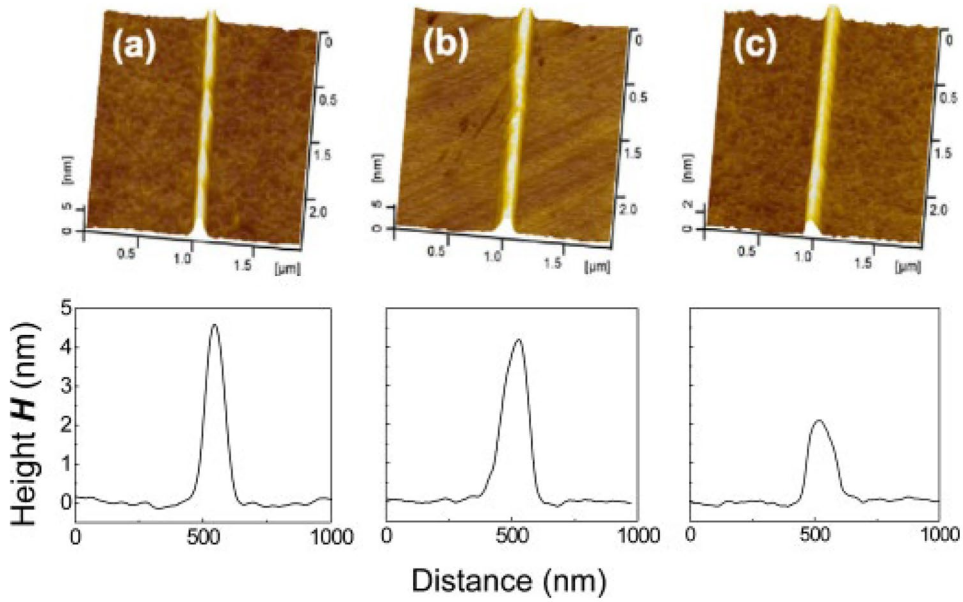

Fig. 45 Comparison of hillocks on different materials created by N = 200 and Fn = 50 μN. (**a**) Si(100), (**b**) monocrystalline quartz and (**c**) glass [140]

the Flower–Nordheim field emission and achieve the effect of the pattern exposure, as shown in Figs. 53 and 54 [169, 196–199, 201–203].

Based on the research results and recent discoveries above, the research directions of nanocutting can be proceed from three aspects as following:

(1) In the nanocutting process, the wear between the tool and the workpiece has a direct impact on the machining surface accuracy and tool life. Therefore, the friction mechanism in the nanocutting process also needs to be studied in depth. The tool is usually regarded as a rigid body in the simulation process, but in the actual process, the impact of tool wear on the machining process is also very significant, so the understanding of the friction and wear behavior and mechanism in the nanocutting process will be further deepened.
(2) Nanoscale cutting by using AFM technology will be an important research direction in the field of nanocutting. However, it still has the problem of low cutting efficiency at the same time. Therefore, the development of high-speed AFM cutting technology is a very challenging direction.
(3) Another direction of nanocutting technology development is the single-atom operation technology. In the single-atom operation method, STM is usually used to realize the movement of a single atom. However, using STM to move a single atom is inefficient, so it is necessary to develop STM technology for moving atoms in large scale by combining various technology from the fields of electricity, magnetism, heat and force.
(4) At this time, the removal mechanism of atoms in atomic scale is still not well understood, which hinders the development of material removal technology in atomic scale. In future, it is necessary to increase the research of the relationship between potential and van der Waals force, electrostatic force and Lorentz force of atoms and to develop new atomic-scale processing technology from the aspect of releasing the interaction force between atoms.

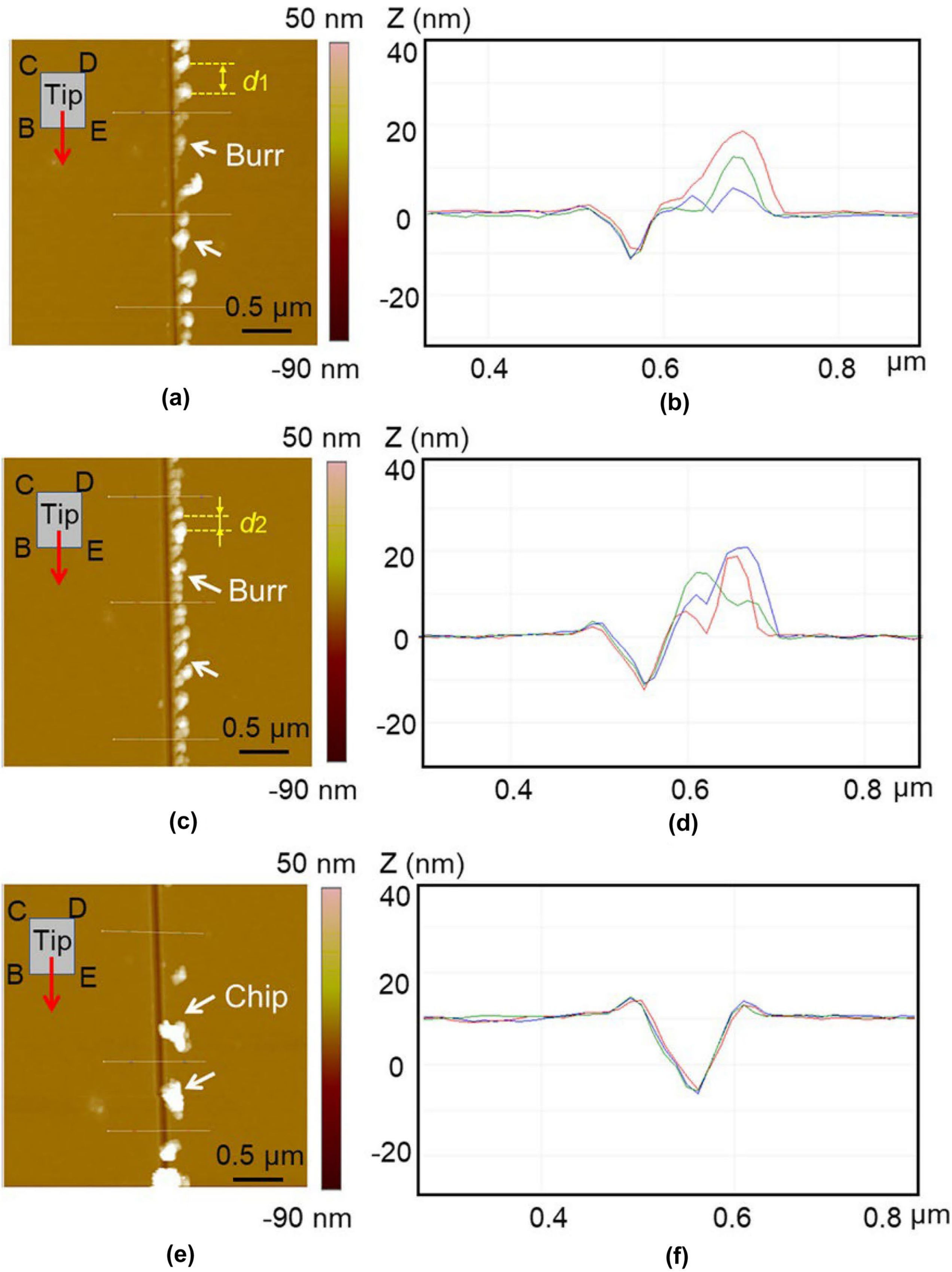

Fig. 46 (**a**,**c**,**e**) Typical AFM images and (**b**,**d**,**f**) cross sections of nanochannels fabricated using normal load of 27 µN, 30 µN and 33 µN, respectively [141]

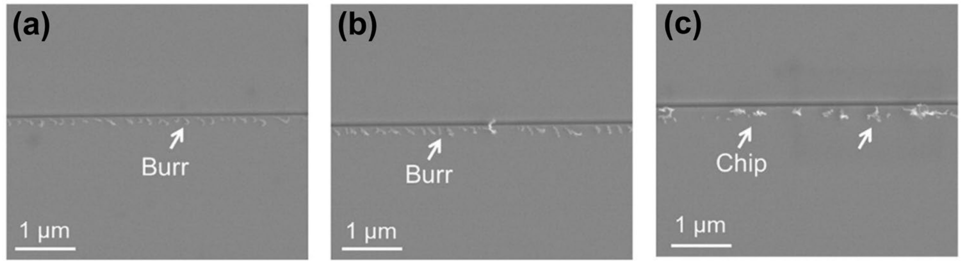

Fig. 47 SEM images of the machined nanochannels for different normal loads: (**a**) 27 μN, (**b**) 30 μN, (**c**) 33 μN [141]

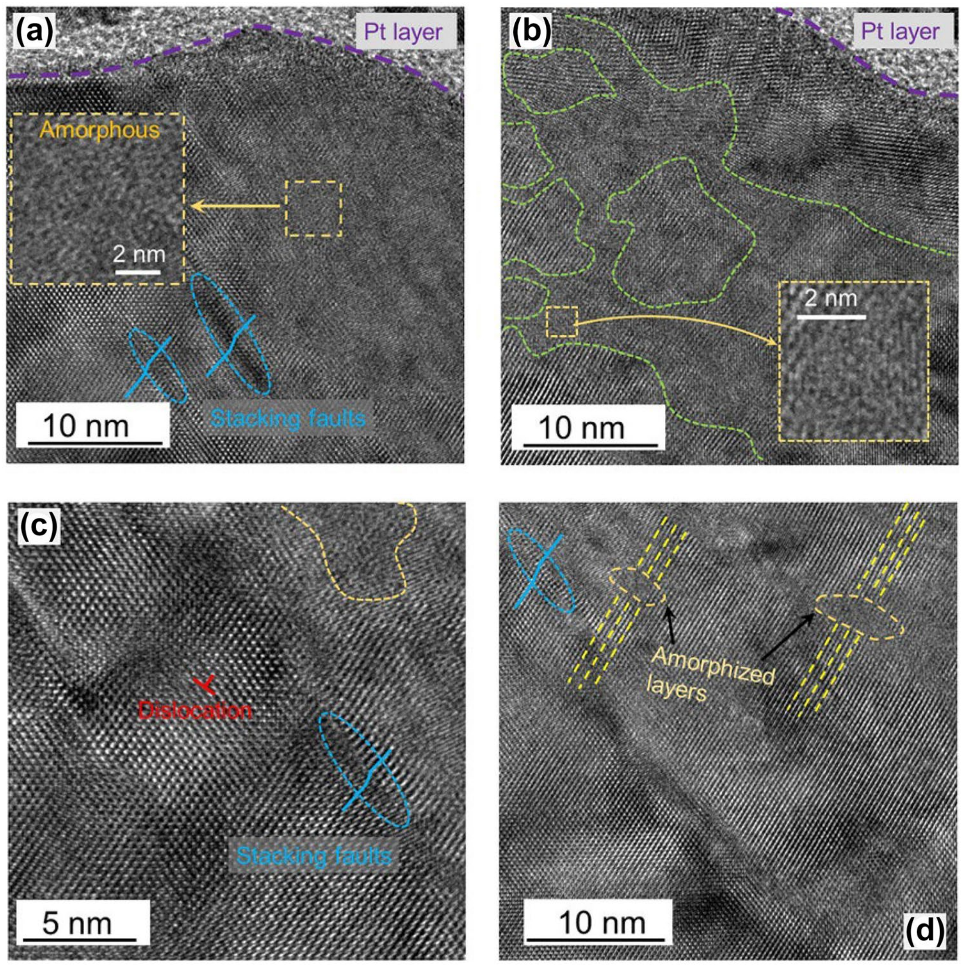

Fig. 48 (**a**)-(**d**) HRTEM images of regions 1, 2, 3 and 4 marked in Fig. 10(**a**). Stacking faults can be observed in (**a**), (**c**) and (**d**). Furthermore, (**b**) and (**d**) show nanocrystallines and amorphized layers, respectively [141]

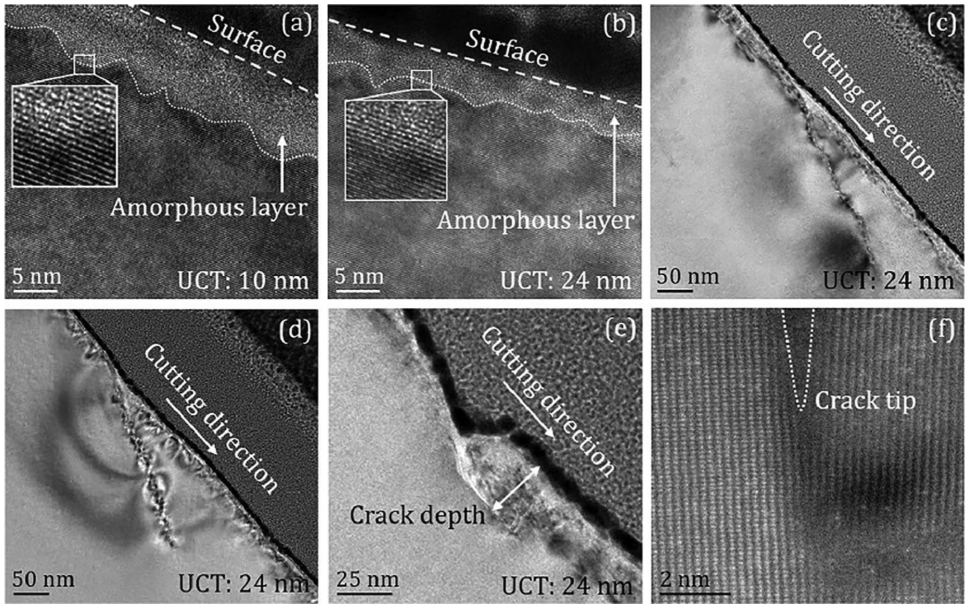

Fig. 49 TEM observations of the (**a**), (**b**) amorphous layer, (**c**), (**d**) linear deformation zone and (**e**), (**f**) nanometric crack in the subsurface. The white spots in the high angle annular dark field image (**f**) are silicon atoms [161]

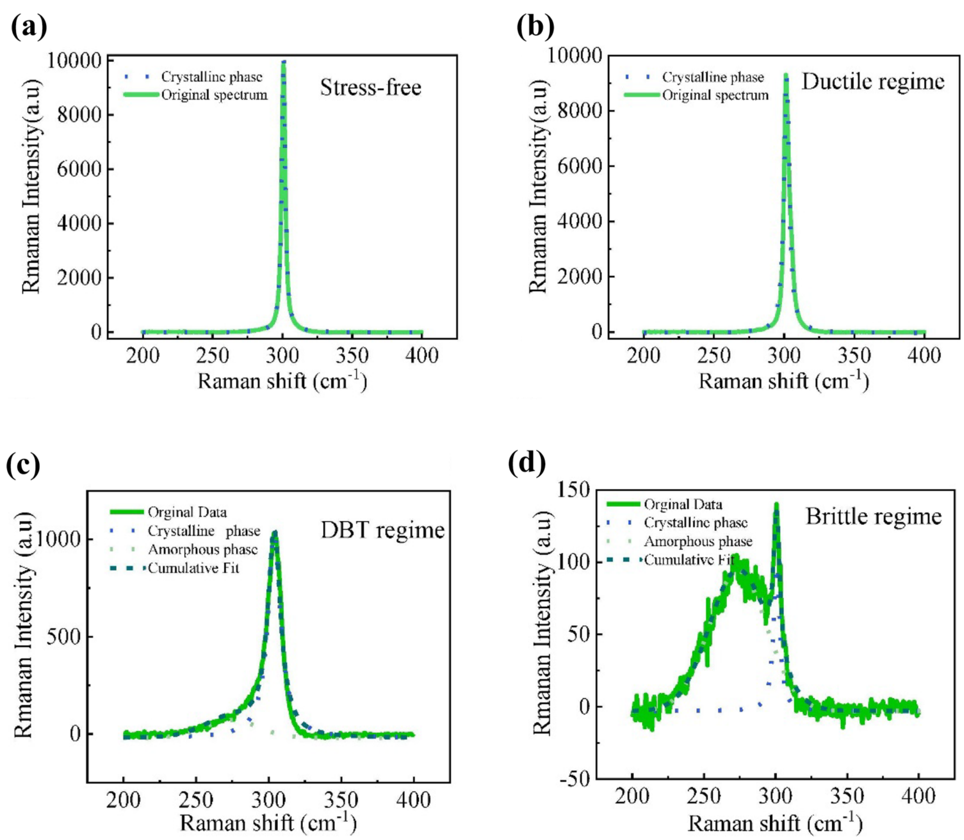

Fig. 50 Raman spectra of: (**a**) original surface, (**b**) ductile regime, (**c**) DBT regime, and (**d**) brittle regime in the varied-load scratch tests [163]

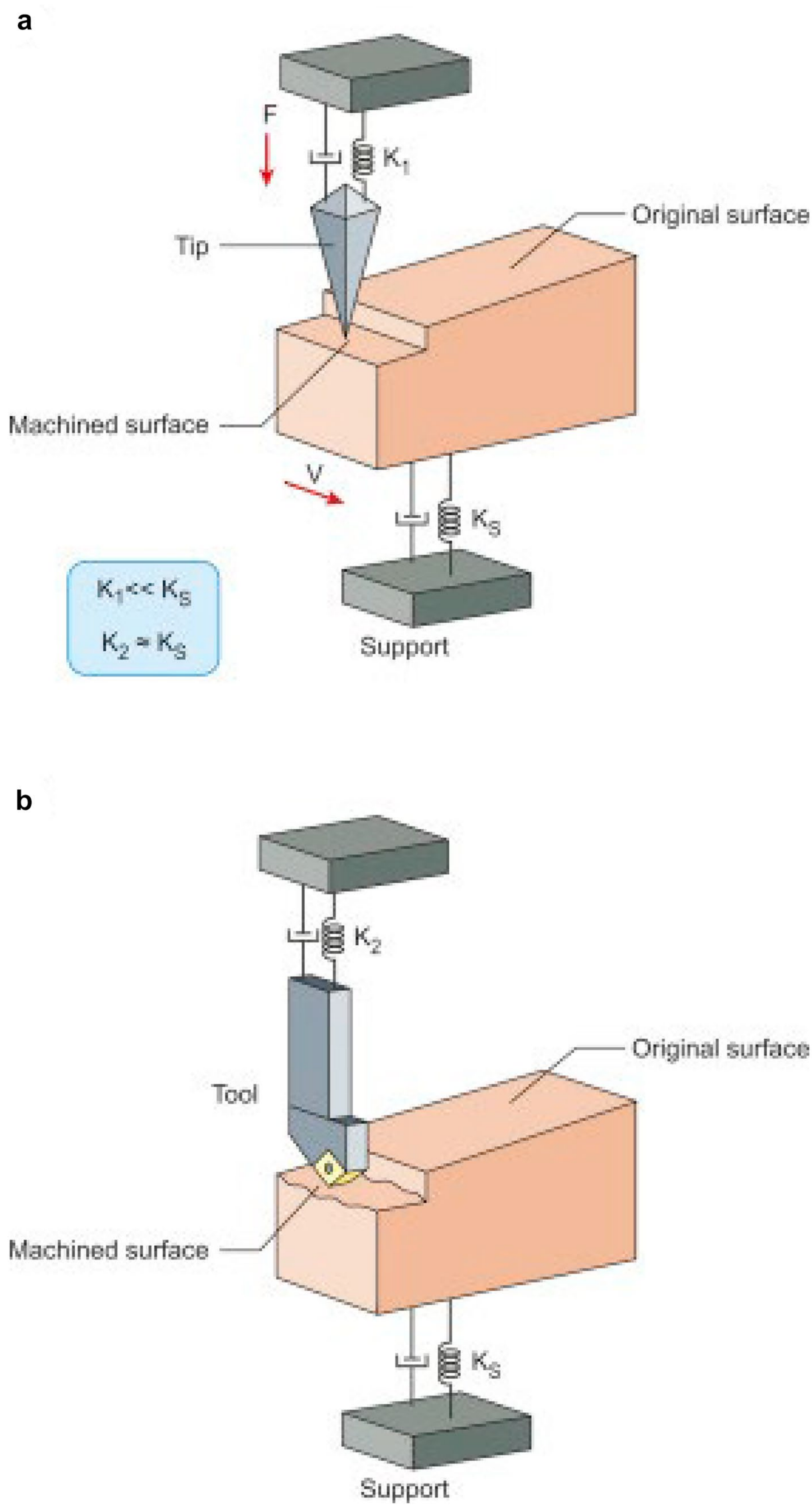

Fig. 51 Schematic of the AFM tip-based nanomechanical machining system. (**b**) Schematic of the conventional cutting system. *K*1 is the elastic constant of the AFM cantilever. *K*2 is the equivalent elastic constant of the tool system. *K*s is the equivalent elastic constant of the support of the machine tools [171]

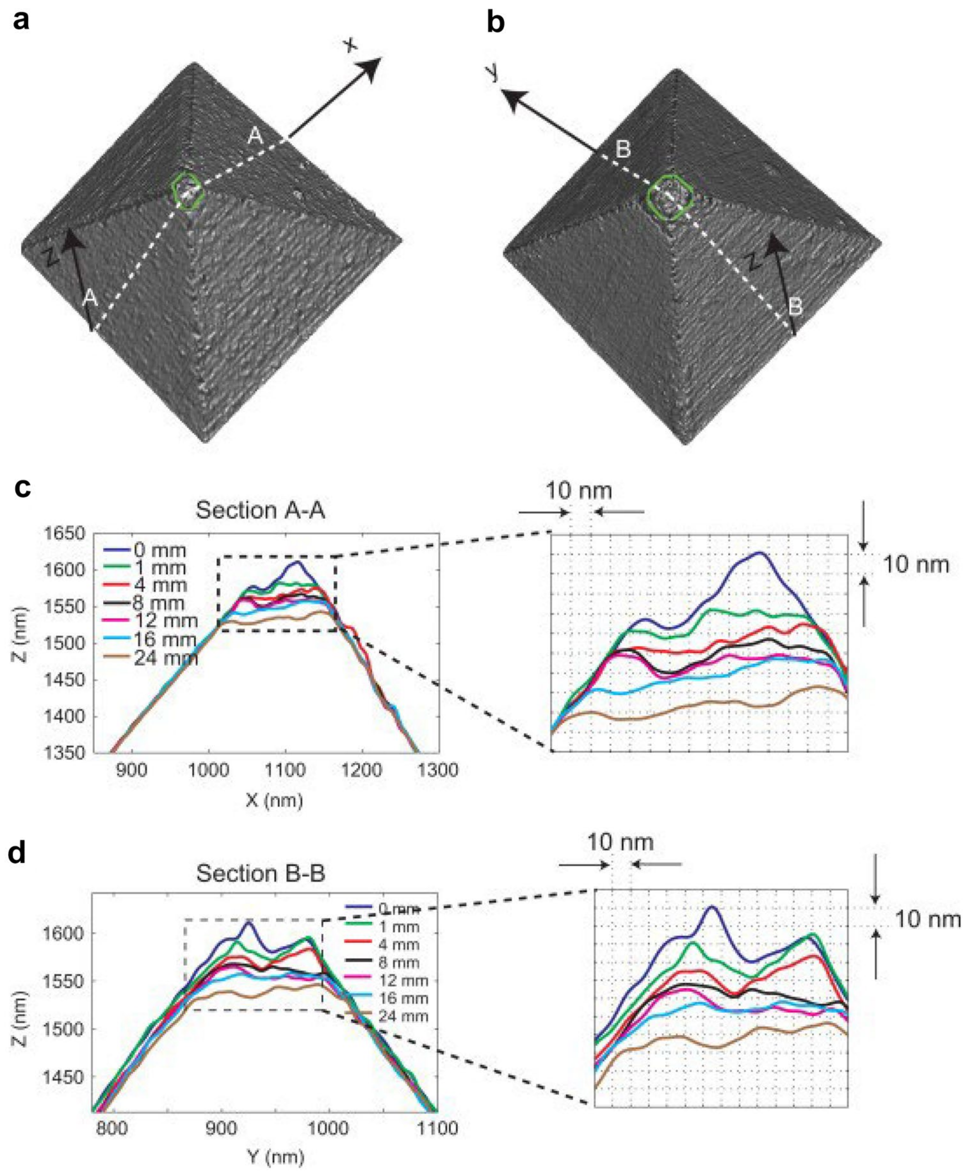

Fig. 52 AFM images obtained at different stages of Test 1 conducted on the silicon samples: (**a**) 3D AFM image of the unworn nanotool, (**b**) 3D AFM image of the nanotool after a total nanomilling distance of 24 mm, (**c**) cross-sectional AFM data from section A–A at different stages of the experiment and (**d**) cross-sectional AFM data from section B–B at different stages of the experiment [168]

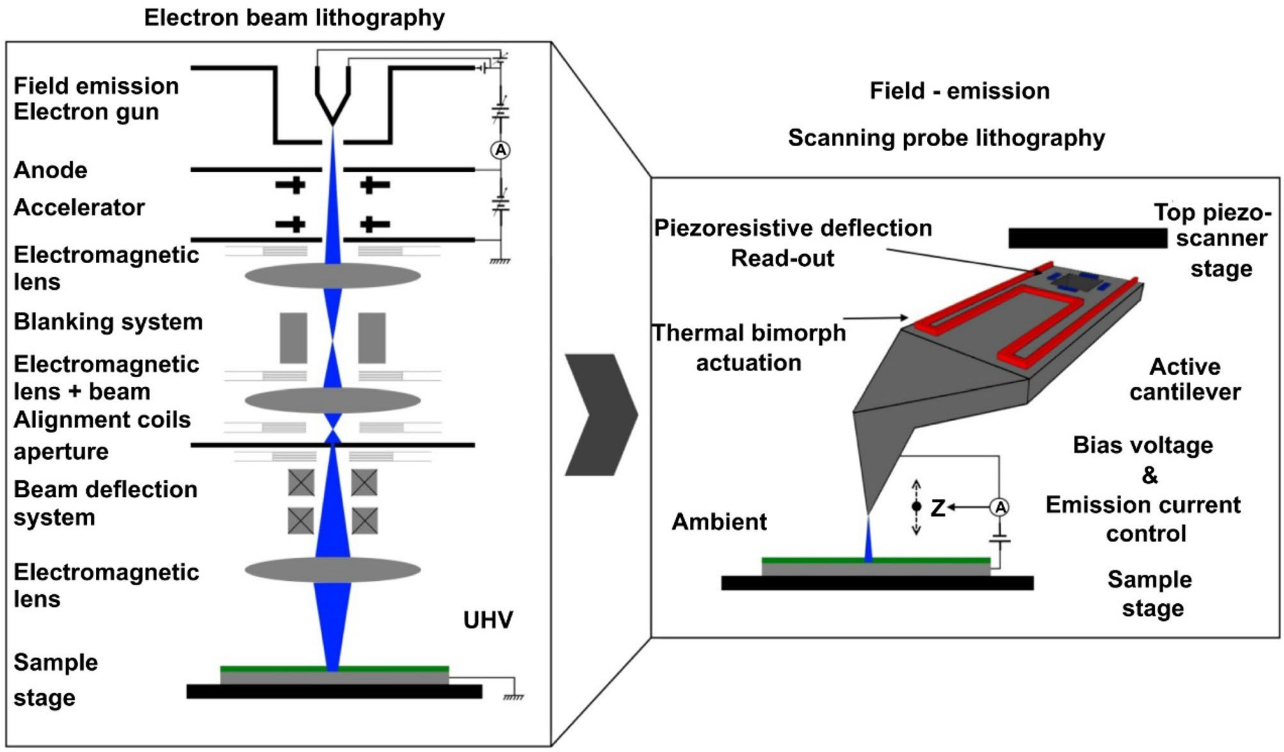

Fig. 53 From classical electron beam lithography (EBL) toward a novel field-emission scanning probe lithography (FE-SPL) system with so-called active cantilever. These cantilevers are equipped with piezoresistive bending senor, a thermomechanical actuator and a sharp tip. In this manner, lithography and imaging are employed using the same cantilever [169]

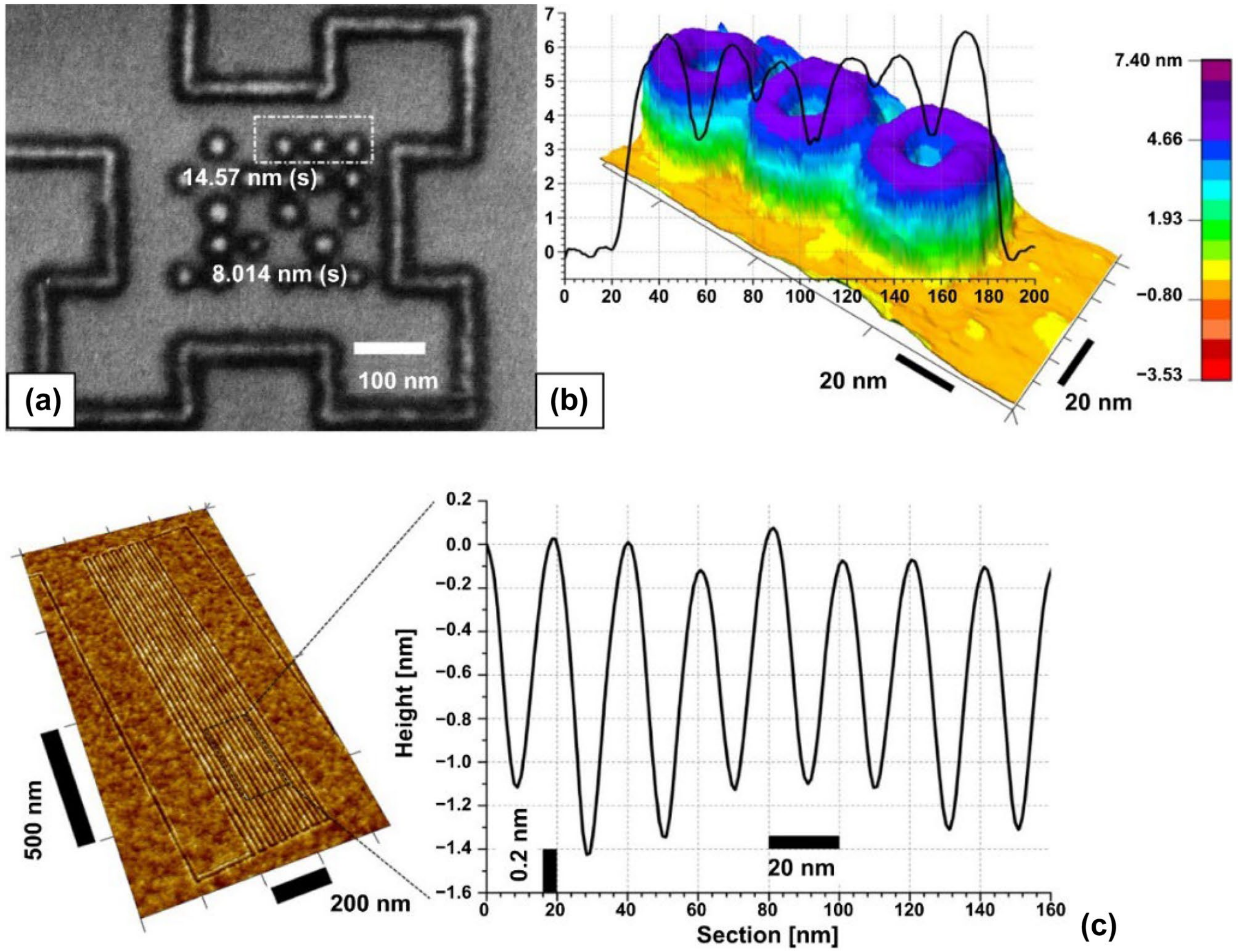

Fig. 54 Donut-like features formed by a superimposed centered ablation of resist with surrounding crosslinking, measured after a wet development step. The spot exposure test array was imaged by SEM (**a**) and AFM (**b**). The donut features were induced by a single-spot exposure FE-SPL process (AFM topographic image and section graphs were not tip-convolution corrected). (**c**) AFM image showing a fragment of test 1.4-mm-long features exposed without interrupting of the exposure process [169]

9 Conclusions

The paper reviews cutting mechanism, tool wear mechanism, subsurface damage mechanism, cutting force, friction force, friction coefficient and nanocutting experiment in the nanocutting process and discusses all aspects from base theories and phenomena. In addition, the challenges and prospects of nanocutting technology are puts forward, and the views are summarized at the end. Meantime, it is believed that nanocutting technology still has certain shortcomings in terms of scale and efficiency. The conclusions are summarized as follows:

(1) The nanomanufacturing technology has widespread influence on the applications of metamaterials, optics, mechanics, quantum devices, 2D materials, nanochannels and nanoconstrictions, which shows that nanomanufacturing is a basic and key technology for the development of other technologies.
(2) The ratio of cutting depth to cutting edge radius (defined as the relative sharpness of the tool, RTS) is a key factor to realize nanocutting. And by increasing the depth of cut when the RTS is unchanged, the primary deformation zone (PDZ) area will also increase and will lead to an increase in internal defects of the workpiece.
(3) The acquiring of critical cutting depth is decisive for the brittle–plastic transition in the processing of brittle materials, and by increasing the temperature of the cutting materials, the critical cutting depth can be increased, which leads to the reduction of processing difficulty for difficult-to-machine materials such as ceramics.

(4) The materials can be classified to easy-to-cut and difficult-to-cut materials for diamond tools. And the tool wear can be explained from the aspect of chemical reaction. Also, the use of nanocutting fluid can significantly improve the wear performance of the tool. At last, the friction and wear properties of different tool materials are different, so it is important to choose the proper material for the tool.

(5) In the nanocutting process, the subsurface damage is reflected in the form of dislocation, phase transformation, amorphization and crack, and with the cutting depth and cutting distance, increasing the subsurface damage also changed and increased. Then, the RDF (radial distribution function) can also be used to characterize the subsurface crystal structure changes.

(6) The cutting force has significant influence on the surface quality of the machining workpieces, so in order to achieve high-efficiency ultraprecision processing, it is necessary to control the cutting force and keep it relatively stable.

(7) The material machinability can be judged by the friction force and the friction coefficient. And the friction coefficient of the material can be acquired by experiment and established analytical formula.

(8) The nanocutting experiments can be implemented in ultraprecision machine tools and nanoscratch instrument, and by the use of cutting force detector, transmission electron microscope (TEM), Raman spectroscopy, in which the cutting force, cutting morphology and subsurface phase change can be acquired.

(9) The wear between the tool and the workpiece has a direct impact on the machining surface accuracy and tool life for ultraprecision machining method. So the research of enhancing the ability of wear resistance for the tool is expected to be further deepened. Also the development of high-speed AFM cutting technology is a very challenging direction. At last, it is necessary to develop STM technology for moving atoms in large scale by combining various technologies from the fields of electricity, magnetism, heat and force. From this aspect, the field emission scanning probe lithography system is a feasible method to solve the problem of current nanomanufacturing technology.

Author contribution Chen Dongju contributed to resources and advisory. Wu Shuiyuan was involved in conceptualization, methodology and writing original draft. Yazhong He, Luo Yuchi and Wang Xiang contributed to review, editing and supervision.

Funding This research was funded by the National Natural Science Foundation of China Grant No.51875005.

Availability of data and material The authors confirm that the data supporting the findings of this study are available within the article. Derived data supporting the findings of this study are available from the corresponding author on request.

Declarations

Ethical approval All authors confirm that they follow all ethical guidelines.

Consent to participate The authors declare that they consent to participate this paper.

Consent to publish The authors declare that they consent to publish this paper and agree with the publication.

Conflicts of interest The authors declare no competing interest.

References

1. Jumare AI, Abou-El-Hossein K, Abdulkadir LN (2017) Review of ultra-high precision diamond turning of silicon for infrared optics. PONTE Int Sci Res J 2017,73 (11) :58–123
2. Zhang SJ, To S, Zhang GQ, Zhu ZW (2015) A review of machine-tool vibration and its influence upon surface generation in ultra-precision machining. Int J Mach Tools Manuf 91:34–42
3. Dong KO, Jeong H, Kim J, Kim I, Jong G, Rho J (2021) Top-down nanofabrication approaches toward single-digit-nanometer scale structures. J Mech Sci Technol 35(3):837–859
4. Zhang J, Cui T, Ge C, Sui Y, Yang H (2016) Review of micro/nano machining by utilizing elliptical vibration cutting. Int J Mach Tools manuf 106:109-126
5. Sun XZ, Cheng K (2010) Micro-/nano-machining through mechanical cutting
6. Zhang ZY, Yan JW, Kuriyagawa T (2019) Manufacturing technologies toward extreme precision. Int J of Extreme Manuf 1(2):19
7. Dong ZX, Wejinya UC (2012) Atomic force microscopy based repeatable surface nanomachining for nanochannels on silicon substrates. App Surf Sci 258 (22) : 8689–8695
8. Gao L, Shigeta K, Guardado AV, Progler CJ, Bogart GR, Rogers JA, Chanda D (2014) Nanoimprinting techniques for large-area three-dimensional negative index metamaterials with operation in the visible and telecom bands. ACS Nano 8(6):5535–5542
9. Mao YT, Kuo KC, Tseng CE, Huang JY, Lai YC, Yen JY, Lee CK, Chuang WL (2009) Research on three dimensional machining effects using atomic force microscope. Rev Sci Instrum 80(6):6797
10. Lee WB, Kong LB, Cheung CF, To S, Chen X, Liu Q (2013) An overview of ultra-precision diamond machining of microstructured freeform surfaces. J Mech Eng 49(19):144
11. Emboras A, Niegemann J, Ma P, Haffner C, Pedersen A, Luisier M, Hafner C, Schimmel T, Leuthold J (2015) Atomic scale plasmonic switch. Nano Lett 16(1):709–714
12. Feng J, Liu K, Graf M, Lihter M, Bulushev RD, Dumcenco D, Alexander DTL, Krasnozhon D, Vuletic T, Kis A, Radenovic A (2015) Electrochemical Reaction in Single Layer MoS2: Nanopores Opened Atom by Atom. Nano Lett 15(5):3431–3438
13. Park H, Shin GH, Lee KJ, Choi SY (2018) Atomic-scale etching of hexagonal boron nitride for device integration based on two-dimensional materials. Nanoscale 10 (32) :15205–15212

14. Yan YD, Geng YQ, Hu ZJ, Zhao XS, Yu BW, Zhang Q (2014) Fabrication of nanochannels with ladder nanostructure at the bottom using AFM nanoscratching method. Nanoscale Res Lett 9(1):212
15. Huang JC, Weng YJ (2014) The study on the nanomachining property and cutting model of single-crystal sapphire by atomic force microscopy. Scanning 36(6):599–607
16. Dong S (2004) Nontraditional manufacturing technique-Nano machining technique based on SPM. Science in China Ser. G Physics
17. Tseng AA, Shirakashi JI, Nishimura S, Miyashita K, Li Z (2010) Nanomachining of permalloy for fabricating nanoscale ferromagnetic structures using atomic force microscopy. J Nanosci Nanotechnol 10(1):456
18. Gao S, Huang H (2017) Recent advances in micro- and nano-machining technologies. Front Mech Eng 12:1–15
19. Fang FZ, Zhang XD, Gao W, Guo YB, Byrne G, Hansen HN (2017) Nanomanufacturing-Perspective and applications. CIRP Ann Manuf Technol 66 (2) :683–705
20. Wang JQ, Yan YD, Li ZH, Geng YQ (2021) Towards understanding the machining mechanism of the atomic force microscopy tip-based nanomilling process. Int J Mach Tools and Manuf.
21. Wang YQ, Tang S, Guo J (2020) Molecular dynamics study on deformation behaviour of monocrystalline GaN during nano abrasive machining. App Surf Sci 510:145492
22. Tsui KH, Lin QF, Chou HT, Zhang QP, Fu HY, Qi PF, Fan ZY (2014) Low-cost, flexible, and self-cleaning 3D nanocone anti-reflection films for high-efficiency photovoltaics. Adv Mat 26 (18) :2805–2811
23. Fang FZ, Zhang N, Guo DM, Ehmann K, Cheung B, Liu K, Yamamura K (2019) Towards Atomic and Close-to-Atomic Scale Manufacturing. Int J Extreme Manuf
24. Zong WJ, Li ZQ, Sun T, Cheng K, Li D, Dong S (2010) The basic issues in design and fabrication of diamond-cutting tools for ultra-precision and nanometric machining. Int J Mach Tools Manuf 50(4):411–419
25. Fang FZ, Wu H, Liu YC (2005) Modelling and experimental investigation on nanometric cutting of monocrystalline silicon. Int J Mach Tools Manuf 45(15):1681–1686
26. Leung TP, Lee WB, Lu XM (1998) Diamond turning of silicon substrates in ductile-regime. J Mater Process Technol 73(1–3):42–48
27. Wang H, Riemer O, Rickens K, Brinksmeier E (2016) On the mechanism of asymmetric ductile-brittle transition in microcutting of (111) CaF2 single crystals. Scripta Materialia 114:21–26
28. Wang ZF, Zhang JJ, Li G, Xu ZW, Zhang HJ, Zhang JG, Hartmaier A, Fang FZ, Yan YD, Sun T (2020) Anisotropy-Related Machining Characteristics in Ultra-Precision Diamond Cutting of Crystalline Copper. Nanomanuf Metrol 3:123–132
29. Liu Q, Liao ZR, Axinte D (2020) Temperature effect on the material removal mechanism of soft-brittle crystals at nano/micron scale. Int J Mach Tools Manuf 159:103620
30. Kalkhoran S, Vahdati M, Yan J (2019) Molecular Dynamics Investigation of Nanometric Cutting of Single-Crystal Silicon Using a Blunt Tool. JOM: the journal of the Minerals, Metals & Materials Society (TMS) 71 (12) :4296–4304
31. Kovalchenko AM (2013) Studies of the ductile mode of cutting brittle materials (A review). J Superhard Mater 35(5):259–276
32. Narulkar R, Bukkapatnam S, Raff L M, Komandun R (2008) Molecular dynamics simulations of diffusion of carbon into iron. Philos Mag 88:1259–1275
33. Kim CJ, Mayor R, Ni J (2012) Molecular dynamics simulations of plastic material deformation in machining with a round cutting edge. Int J Precision Eng Manuf 13(8) :p.1303–1309
34. Abdulkadir LN, Bello AA, Bawa MA, Abioye AM (2020) Nanometric behaviour of monocrystalline silicon when single point diamond turned-a molecular dynamics and response surface methodology analysis. Eng Res Exp 2(3):035038
35. Bai QS, Liang YC, Li DG, Yang CL (2006) Molecular Dynamics Simulation of Nanometric Machining. Micro Technol (04):57–62
36. Wang J, Zhang XD, Fang FZ, Xu FF, Chen RT, Xue ZF (2020) Study on nano-cutting of brittle material by molecular dynamics using dynamic modeling. Comput Mat Sci 183:109851
37. Zhang L, Zhao H, Ma Z, Huang H, Shi C, Zhang W (2012) A study on phase transformation of monocrystalline silicon due to ultra-precision polishing by molecular dynamics simulation. AIP Adv 2(4):860
38. Zhang P, Gao X, Zhang XC, Wang YQ (2020) Effects of cutting parameters on the subsurface damage of single crystal copper during nanocutting process. Vacuum
39. Xie W, Fang F (2020) Effect of tool edge radius on material removal mechanism in atomic and close-to-atomic scale cutting. App Surf Sci 504 (6064) :144451
40. Wang PC, Yu JG, Zhang QX (2020) Nano-cutting mechanical properties and microstructure evolution mechanism of amorphous/single crystal alloy interface. Comput Mat Sci 184:109915
41. Liu H, Guo YB, Zhao PY (2020) Surface generation mechanism of monocrystalline materials under arbitrary crystal orientations in nano cutting. Mater Today Commun 25:101505
42. Wang QL, Zhang CF, Wu MP, Chen JX (2020) Effect of Fluid Media on Material Removal and Subsurface Defects Evolution of Monocrystal Copper in Nano-Cutting Process. Nano research letters.
43. Liu B, Xu ZW, Chen C, Li R, Gao X, Liang L (2020) Numerical and experimental investigation on ductile deformation and subsurface defects of monocrystalline silicon during nano-scratching. App Surf Sci 528:147034
44. Chen CH, Lai M, Fang FZ (2021) Subsurface deformation mechanism in nano-cutting of gallium arsenide using molecular dynamics simulation. Nanoscale Res Lett 16,117
45. Zhu B, Zhao D, Zhao HW, Guan J, Hou PL, Wang SB, Qian L (2017) A study on the surface quality and brittle–ductile transition during the elliptical vibration-assisted nanocutting process on monocrystalline silicon via molecular dynamic simulations. RSC Adv 7(7):4179–4189
46. Zhao PY, Wu JW, Chen HF, Liu H, Li D, Tan JB (2021) Molecular dynamics simulation study of interaction mechanism between grain boundaries and subgrain boundaries in nano-cutting. J Manuf Process 67:418–426
47. Antwi EK, Liu K, Wang H (2018) A review on ductile mode cutting of brittle materials. Front Mech Eng 13(2) :251–263
48. Xiao GB, To S, Zhang GQ (2015) Molecular dynamics modelling of brittle-ductile cutting mode transition: case study on silicon carbide. Int J Mach Tools Manuf 88:214–222
49. Suryam LV, Pradeep AV, Prasad SVS, Kumari PP (2019) Functioning mechanism of nanomaterials and significance on machinability: A review. Mater Today Proc 19:560–563
50. Kalkhoran SA, Vahdati M (2019) The effect of interatomic potential function on nanometric machining of single crystal silicon. J App Comput Sci Mech 30(2)
51. Liu H, Guo YB, Li D, Wang JQ (2021) Material Removal Mechanism of FCC Single-crystalline Materials at nano-scales: Chip Removal & Ploughing. J Mat Process Technol 294:117106
52. Chen YH, Han H, Fang FZ, Hu XT (2014) MD simulation of nanometric cutting of copper with and without water lubrication. SCIENCE CHINA Technol Sci 57(006):1154–1159
53. Lai M, Zhang XD, Fang FZ, Bi MH (2017) Fundamental investigation on partially overlapped nano-cutting of monocrystalline germanium. Prec Eng 49: 160
54. Ng CK, Melkote SN, Rahman M, Kumar AS (2006) Experimental study of micro- and nano-scale cutting of aluminum 7075–T6. Int J Mach Tools Manuf 46(9):929–936

55. Markopoulos AP, Karkalos NE, Papazoglou EL (2020) Meshless Methods for the Simulation of Machining and Micro-machining: A Review. Arch Comput Methods Eng 27(3):831–853
56. Sun X, Kai C (2010) Multi-scale simulation of the nano-metric cutting process. The Int J Adv Manuf Technol 47 (9–12)
57. Pen HM, Liang YC, Luo XC, Bai QS, Goel S, Ritchie JM (2011) Multiscale simulation of nanometric cutting of single crystal copper and its experimental validation. Comput Mat Sci
58. Sun XZ, Chen SJ, Cheng K, Huo DH, Chu WJ (2006) Multiscale simulation on nanometric cutting of single crystal copper. Proc Inst Mech Eng B J Eng Manuf 220(7):1217–1222
59. Chen CH, Lai M, Fang FZ (2021) Subsurface Deformation Mechanism in Nano-cutting of Gallium Arsenide Using Molecular Dynamics Simulation. Nano Research Letters 16(1):1–10
60. Khatri N, Garg H, Karar V (2018) Experimental and simulation study of nanometric cutting of silicon by diamond turning. Materials Today: Proceedings.
61. Romero PA, Anciaux G, Molinari A, Molinari JF (2012) Friction at the tool-chip interface during orthogonal nanometric machining. Model Simul Mat Sci Eng 20 (5) :55007–55022
62. Liu H, Guo YB, Zhao PY (2020) Surface generation mechanism of monocrystalline materials under arbitrary crystal orientations in nanoscale cutting. Mat Today Commun 25:101505
63. Zhang P, Zhang XC, Yu X, Wang YQ (2020) Research on the nanocutting mechanism of Ni-Fe-Cr-based superalloys: Conventional cutting versus UEVC. Mater Today Commun 26 (11) :101795
64. Van Bouwelen FM, Field JE, Brown LM (2003) Electron microscopy analysis of debris produced during diamond polishing. Philos Mag A 83(7):839–855
65. Zhao QL, Chen MJ, Liang YC, Dong S (2002) Wear of Diamond Cutting Tool in Ultra-precision Single Point Turning. Tribology 22(005):321–327
66. Liang YC, Guo YB, Chen MJ (2008) New Progress of Research in Diamond Tool Wear of Nanometric Machining. Mocaxue Xuebao/Tribology 28(3):282–288
67. Robinson GM, Jackson MJ, Whitfield M (2007) A review of machining theory and tool wear with a view to developing micro and nano machining processes. J Mater Sci 42(6):2002–2015
68. Zhang SJ, To S, Zhang GQ (2017) Diamond tool wear in ultra-precision machining. Int J Adv Manuf Technol 88(1–4):1–29
69. Tseng AA (2011) Advancements and challenges in development of atomic force microscopy for nanofabrication. Nano Today 6(5):493–509
70. Wu ZH, Liu WD, Zhang LC (2017) Revealing the deformation mechanisms of 6H-silicon carbide under nano-cutting. Comput Mat Sci
71. Kilincarslan E, Kilincarslan SK, Cetin MH (2021) Evaluation of the Clean Nano-cutting Fluid by Considering the Tribological Performance and Cost Parameters. Tribology Int 157:106916
72. Fang FZ, Xu FF (2018) Recent Advances in Micro/Nano-cutting: Effect of Tool Edge and Material Properties. Nanomanuf Metrol
73. Cheng K, Luo X, Ward R, Holt R (2003) Modeling and simulation of the tool wear in nanometric cutting. Wear 255(7):1427–1432
74. Wang ZF, Sun T, Zhang HJ, Li G, Li ZQ, Zhang JJ, Yan YD, Hartmaier A (2019) The interaction between grain boundary and tool geometry in nanocutting of a bi-crystal copper. Int J of Extreme Manuf 1(4):11
75. Cui DD, Zhang LC (2017) Nano-machining of materials: understanding the process through molecular dynamics simulation. Adv manuf
76. Zhu Y, Hui-Ting MA, Fan H (2018) Effect of tool wear on the nano-cutting process of single crystal aluminum. J Mach Tools Man
77. Khalil ANM, Azmi AI, Murad MN, Ali MAM (2018) The effect of cutting parameters on cutting force and tool wear in machining Nickel Titanium Shape Memory Alloy ASTM F2063 under Minimum Quantity Nanolubricant. Procedia CIRP
78. Wang ZG, Liang YC, Chen MJ, Tong Z, Chen JX (2010) Analysis about diamond tool wear in nano-metric cutting of single crystal silicon using molecular dynamics method. Proc SPIE
79. Kuai JC, Zhang FH (2011) Friction,wear and cutting performances of nano cemented carbide cutter. Tribology
80. Mukhtar NFH (2017) Characterisation of tip wear during AFM probe-based nanomachining
81. Singh G, Mishra V, Karar V, Banwait SS (2019) Diamond Tool Wear Measurement by Profilometry Method for Ultra-precision Machining of Silicon. Mater Today Commun
82. Bushlya V, Lenrick F, Bjerke A, Aboulfadl H, Thuvander M, Stahl JE, Saoubi RM (2021) Tool wear mechanisms of PcBN in machining Inconel 718: analysis across multiple length scale. CIRP Annals
83. Zhang P, Cao X, Zhang XC, Wang YQ (2021) Effects of cutting parameters on the subsurface damage of single crystal copper during nanocutting process. Vacuum 187:109420
84. Zhao PY, Zhang Q, Guo YB, Liu H, Deng ZQ (2020) Atomistic simulation study of nanoparticle effect on nano-Cutting mechanisms of single-crystalline materials. Micromachines 11(3):265
85. Liu L, Xu ZW, Tian DY, Hartmaier A, Luo XC, Zhang JJ, Nordlund K, Fang FZ (2019) MD simulation of stress-assisted nanometric cutting mechanism of 3C silicon carbide. Tribology 71(5):686–691
86. Li ZH, Yan YD, Wang JQ, Geng YQ (2020) Molecular Dynamics Study on Tip-Based Nanomachining: A Review. Nano research letters 15(1):1–12
87. Zhang JJ, Zhang JG, Wang ZF, Hartmaier A, Yan YD, Sun T (2017) Interaction between phase transformations and dislocations at incipient plasticity of monocrystalline silicon under nanoindentation. Comput Mater Sci 131:55–61
88. Gao Y, Urbassek HM (2014) Evolution of plasticity in nanometric cutting of Fe single crystals. Appl Surf Sci 317:6–10
89. Chen X, Liu CL, Ke JY, Zhang JG, Shu XW, Xu JF (2020) Subsurface damage and phase transformation in laser-assisted nanometric cutting of single crystal silicon. Materials & Design 190: 108524
90. Zhao H, Shi C, Zhang P et al (2012) Research on the effects of machining-induced subsurface damages on mono-crystalline silicon via molecular dynamics simulation. Appl Surf Sci 259:66–71
91. Zw A, Wl A, Lz A et al (2020) Amorphization and dislocation evolution mechanisms of single crystalline 6H-SiC. Acta Mater 182:60–67
92. Wang J, Zhang X, Fang F, Chen R (2018) A numerical study on the material removal and phase transformation in the nanometric cutting of silicon. Appl Surf Sci
93. Liu HT, Hao MJ, Tao MF, Sun YZ, Xie WK (2019) Molecular dynamics simulation of dislocation evolution and surface mechanical properties on polycrystalline copper. Appl Phys A 125(3)
94. Wang QL, Zhang CF, Wu MP, Chen JX (2019) Subsurface Crystal Structural Evolution Mechanism of Single Crystal Coppers during Nano-indentation. Chin J Mech Eng
95. Chen C, Lai M, Fang F (2021) Study on the crack formation mechanism in nano-cutting of gallium arsenide. App Surf Sci 540:148322
96. Huang N, Yan Y, Zhou P, Kang RK, Guo DM (2019) Elastic-plastic deformation of single-crystal silicon in nano-cutting by a single tip tool. Japanese J App Phys.
97. Zhou P, Sun T, Shi X D, Li J, Zhu YW, Wang ZK (2019) Atomic-scale study of vacancy defects in SiC affecting on removal mechanisms during nano-abrasion process. Tribology Int 145:106136

98. Wang QL, Bai QS, Chen JX, Sun YZ, Guo YB, Liang YC (2015) Subsurface defects structural evolution in nano-cutting of single crystal copper. App Surf Sci 344:38–46
99. Wang QL, Wu MP, Zhang CF, Lv YM, Ji XG (2019) Effect of machining-induced subsurface defects on dislocation evolution and mechanical properties of materials via nano-indentation. Nano Res Lett 14(1)
100. Morozov IA (2021) Atomic force microscopy nanoindentation kinetics and subsurface visualization of soft inhomogeneous polymer. Microsc Res Tech 84(9)
101. Woste F, Kimm J, Bergmann JA, Theisen W, Wiederkehr P (2021) Investigation of the effect of residual stresses in the subsurface on process forces for consecutive orthogonal cuts. Prod Eng
102. Yan YY, Zhang YF, Zhao B, Liu JL (2021) Surface formation and damage mechanisms of nano-ZrO_2 ceramics under axial ultrasonic-assisted grinding. J Mech Sci Technol 35(3):1187–1197
103. Zhang HL, Ji-Cai K, Zhang FH (2010) Minimum Thickness of Cut in Nanomachining Using Atomic Force Microscopy. IEEE
104. Lai M, Zhang XD, Fang FZ, Bi MH (2019) Effects of crystallographic orientation and negative rake angle on the brittle-ductile transition and subsurface deformation in machining of monocrystalline germanium. Prec Eng 56:164–171
105. Diaz OG, Axinte DA, Butler-Smith P, Novovic D (2019) On understanding the microstructure of SiC/SiC Ceramic Matrix Composites (CMCs) after a material removal process. Mater Sci Eng 743:1–11
106. Mester L, Govyadinov AA, Chen S, Goikoetxea M, Hillenbrand R (2020) Subsurface chemical nanoidentification by nano-FTIR spectroscopy. Nat Commun 11(1)
107. Goel S (2014) The current understanding on the diamond machining of silicon carbide. Journal of Physics, D. Applied Physics: A Euro J
108. Chen YL, Chen FW, Li ZW, Zhang Y, Ju BF, Lin HB (2021) Three-axial cutting force measurement in micro/nano-cutting by utilizing a fast tool servo with a smart tool holder CIRP Ann Manuf Technol 70(1) :33–36
109. Kang Q, Fang XD, Sun L, Ding JJ, Jiang ZD (2019) Research on mechanism of nanoscale cutting with arc trajectory for monocrystalline silicon based on molecular dynamics simulation. Comput Mat Sci
110. Lin ZC, Huang JC (2008) The influence of different cutting speeds on the cutting force and strain–stress behaviors of single crystal copper during nano-scale orthogonal cutting. J Mater Process Technol 201(1–3):477–482
111. Lin ZC, Huang JC (2008) A study of the estimation method of the cutting force for a conical tool under nanoscale depth of cut by molecular dynamics. Nanotechnology 19 (11) :115701
112. Goel S, Rashid WB, Luo XC, Agrawal A, Jain VK (2013) A Theoretical Assessment of Surface Defect Machining and Hot Machining of Nanocrystalline Silicon Carbide. J Manuf Sci Eng
113. He Y, Lai M, Fang FZ (2019) A numerical study on nanometric cutting mechanism of lutetium oxide single crystal. App Surf Sci 496:143715
114. Li ZW, Chen YL, Wu L, Ju BF (2021) Development of a force controlled nanocutting system using a flexible mechanism for adaptive cutting of microstructures on non-planar surfaces. Prec Eng 72 (2)
115. Goel S (2013) An atomistic investigation on the nanometric cutting mechanism of hard, brittle materials.
116. Kong XC, Dong JY, Cohen PH (2017) Modeling of the dynamic machining force of vibration-assisted nanomachining process. J Manuf Process 28:101–108
117. Asakura K, Hirohata Y, Suzuki T, Hoshino Y (2004) Development and stress analysis of nano cutting force detector. J Japan Ins Metals 68 (5) :275–281
118. Kong XZ, Zhang L, Dong JY, Cohen PH (2015) Machining force modeling of vibration-assisted nano-machining process
119. Wang JH, Dong S, Wang HX, Chen MJ, Zong WJ, Zhang LJ (2007) Forecasting of surface roughness and cutting force in single point diamond turning for KDP Crystal. Key Eng Mater 339:78–83
120. Lin ZC, Lin CT, Hsu YC (2015) Theoretical model of calculating cutting force and down force for nanocutting of v-shaped groove on single-crystal silicon. J Chin Soc Mech Eng Trans Chin Inst Eng 36(5):363–374
121. Chang WJ, Fang TH, Weng CI (2004) Inverse determination of the cutting force on nanoscale processing using atomic force microscopy. Nanotechnology 15(5):427–430
122. Xu ZW, Liu LF, Jia RL, Guo C (2017) A cutting force detection method based on SEM online nanometric cutting. J Tianjin Univ (Science and Technology)
123. Zhao Y, Li TT, Zhang Y, Huo DH (2017) Effect of machining parameters on the cutting force and microstructure in nanometric cutting of Cu50Zr50 metallic glass. Current Nanosci
124. Kang IS, Kim JS, Yong WS (2008) Cutting force model considering tool edge geometry for micro end milling process. J Mech Sci Technol 22 (2) :293–299
125. Gokhale A, Jain J, Prasad R, Huang EW, Lee SY (2020) Characterization of Deformation and Wear Mechanisms During Indentation Scratching on Pure Zinc. Tribology 142 (1) : 011701
126. Wang ZQ, Jiao ND, Tung S, Dong ZL (2010) Research on the atomic force microscopy-based fabrication of nanochannels on silicon oxide surfaces. Chin Sci Bull 55 (30) :3466–3471
127. Choi DH, Lee JR, Kang NR, Je TJ, Kim JY, Jeon EC (2017) Study on ductile mode machining of single-crystal silicon by mechanical machining. Int J Mach Tools Manuf 113:1–9
128. Islam S, Ibrahim RN (2011) Mechanism of Abrasive Wear in Nanomachining. Tribol Lett 42(3):275–284
129. Harano K, Satoh T, Sumiya H (2012) Cutting performance of nano-polycrystalline diamond. Diam Relat Mater 24:78–82
130. Eltaggaz A, Nouzil I, Deiab I (2021) Machining Ti-6Al-4V Alloy Using Nano-Cutting Fluids: Investigation and Analysis. J Manuf Mater Proc 5(2):42
131. Li Y, Yang XJ (2016) Molecular dynamics simulation of single crystal copper material surface cutting properties in nano-scale. Chin Mech Eng 27 (006) :721–726
132. Chamani HR, Ayatollahi MR (2018) Prediction of friction coefficients in nanoscratch testing of metals based on material flow lines. Theor Appl Frac Mech
133. Babu VVP, Reddy YA (2019) Experimental investigation to study the effects of vegetable oil based nano fluids on cutting forces and surface quality in machining. Int J Res Adv Technol
134. Budnitzki M, Kuna M (2018) Scratching of silicon surfaces. Int J Solids Struc
135. Ekwińska MA, Rymuza Z (2010) New approach to estimate nanowear test results through nanoindentation test. Microelectron Eng 87(5–8):1404–1409
136. Mylvaganam K, Zhang LC (2011) Micro/nano tribology. Tribology
137. Carreon AH, Funkenbusch PD (2018) Material specific nanoscratch ploughing friction coefficient. Tribol Int 126:363–375
138. Yang X, Qiu ZJ, Wang YG (2019) Investigation of material flow behaviour and chip formation mechanism during grinding of glass-ceramics by nanoscratch. Ceram Int 45(13)
139. Elkaseer A, Broussea EB (2013) Modelling the surface generation process during AFM probe-based machining: simulation and experimental validation. Surf Topogr
140. Yu BJ, Dong HS, Qian LM, Chen YF, Yu JX, Zhou ZR (2009) Friction-induced nanofabrication on monocrystalline silicon. Nanotechnol 20 (46) :465303

141. Wang JQ, Yan YD, Jia BS, Geng YQ (2021) Study on the processing outcomes of the atomic force microscopy tip-based nanoscratching on GaAs. J Manuf Proc 70:238–247
142. Gao W, Hocken RJ, Patten JA, Lovinggood J (2000) Experiments using a nano-machining instrument for nano-cutting brittle materials. CIRP Ann Manuf Technol
143. Yang XJ, Luo L (2019) Nano-scratch instrument-based experimental research of single crystal germanium nanogrooves machining. Rare Metal Mat Eng 048 (001) :221–226
144. Geng RW, Yang XJ, Xie QM, Li R, Luo L (2019) Cutting mechanism of monocrystalline germanium based on nano scratch experiment. Rare Metal Mat Eng 397 (08) :156–161
145. Yang XJ, Li Y (2015) Experimental study on the cutting properties of single crystal copper anisotropic surface in micro-nano scale. Materials Reports 29 (008) :95–99
146. Liu B, Xu ZW, Wu W, Wang ZQ (2015) Design and experiment on SEM based nanometric cutting device. J Tianjin University (Science and Technology) 48:56–61
147. Gozen BA, Ozdoganlar OB (2012) Design and evaluation of a mechanical nanomanufacturing system for nanomilling. Prec Eng 36(1):19–30
148. Asakura K, Hirohata Y, Hirasaka M, Nagasawa T, Suzuki T, Hoshino Y (2004) Development and applications of nano-cutting force detector using ultra microtome. kenbikyo 39:C483-C483
149. Sun W, Duan CZ, Yin WD (2021) Chip formation mechanism in machining of Al/SiCp composites based on analysis of particle damage. J Manuf Proc 64:861–877
150. Zhang YF, Li S, Yang XJ, Wu SH, Liu H (2019) Molecular dynamics simulation of monocrystal germanium nanocutting with vacancy defects. J Electron Sci Technol
151. Sharma A, Datta D, Balasubramaniam R (2019) A molecular dynamics simulation of wear mechanism of diamond tool in nano cutting of copper beryllium. J Adv Manuf Technol 102 (1) :731–745
152. Shikimaka O, Prisacaru A (2019) Deformation mechanisms under nanoscratching of Si: effect of scratching speed, load and indenter orientation. Mater Res Exp 6(8) :085011
153. Geng YQ, Yan YD, Brousseau E, Sun YW (2017) AFM tip-based mechanical nanomachining of 3D micro and nanometric structures via the control of the scratching trajectory. J Mech Mater Proc Technol
154. Barkachary BM, Joshi SN (2021) Numerical Computation and Analysis of Cutting Forces during Nanometric Scratching of Silicon Carbide. J Inst Eng India Ser C 1–10
155. Zhang FH, Li C, Min BB, Zhao H, Liu ZD (2016) Investigation of Surface Deformation Characteristic and Removal Mechanism for K9 Glass Based on Varied Cutting-depth Nano-scratch. J Mech Eng 52 (017) :65–71
156. Geng RW, Yang XJ, Xie QM, Li R, Luo L (2019) Material removal mechanism of monocrystalline germanium based on nano-scratch experiment. J Inorganic Mater 34 (8)
157. Yang XJ, Zhao B, Luo L (2018) Experimental research on brittle-ductile transition of single crystal germanium based on nano-scratch. Rare Metal Mater Eng 47(10):314–318
158. Luo L, Yang XJ (2019) Mechanical properties experiment of monocrystalline germanium with multiple scratches based on nano scratch instrument. Chin J Nonferrous Met 029(010):2341–2347
159. Zhu YD, Zhang QL, Zhao QL, To S (2021) The material removal and the nanometric surface characteristics formation mechanism of TiC/Ni cermet in ultra-precision grinding. Int J Refract Hard Met
160. Malshe AP, Rajurkar KP, Virwani KR, Taylor CR, Bourell DL, Levy G, Sundaram MM, McGeough JA, Kalyanasundaram V, Samant AN (2010) Tip-based nanomanufacturing by electrical, chemical, mechanical and thermal processes. CIRP Ann Manuf Technol 59(2):628–651
161. Wang JS, Fang FZ (2021) Nanometric cutting mechanism of silicon carbide. CIRP Annals - Manuf Technol
162. Wang YQ, Li XL, Wu YQ, Mu DK, Han H (2021) The removal mechanism and force modelling of gallium oxide single crystal in single grit grinding and nanoscratching. Int J Mech Sci 204:106562
163. Geng RW, Yang XJ, Xie QM, Xiao JG, Zhang WQ, Li R (2021) Fundamental study on material removal mechanism in single-crystal germanium. Infrared Phys Technol 116:103773
164. Zhan DP, Han LH, Zhang J, He QF, Tian ZW, Tian ZQ (2017) Electrochemical micro/nano-machining: principles and practices. Chem Soc Rev
165. Faisal N, Zindani D, Kumar K (2019) Micro and Nano Machining-An Industrial Perspective
166. An Q, Chen J, Ming WW, Chen M (2020) Machining of SiC Ceramic Matrix Composites: A Review. Chin J Aeronaut
167. Rahman MA, Amrun MR, Rahman M, Kumar AS (2017) Variation of surface generation mechanisms in ultra-precision machining due to relative tool sharpness (RTS) and material properties. Int J Mach Tools Manuf
168. Ozdoganlar OB, Gozen BA (2014) Wear of ultrananocrystalline diamond AFM tips during mechanical nanomanufacturing by nanomilling. Wear
169. Kaestner M, Rangelow I (2020) Scanning Probe Lithography on Calixarene towards Single-Digit Nanometer Fabrication. Int J Extreme Manuf 2(3):21
170. Zhou P, Shi XD, Li J, Sun T, Zhu YW, Wang ZK, Chen JP (2019) Molecular dynamics simulation of SiC removal mechanism in a fixed abrasive polishing process. Ceram Int
171. Yan YD, Geng YQ, Hu ZJ (2015) Recent advances in AFM tip-based nanomechanical machining. International J Mach Tools Manuf
172. Muthuramalingam T (2019) Recent Trends in Micro and Nano Mach Eng Mat
173. Jackson MJ, Robinson GM, Whitfield MD, Ahmed W, Morrell JS (2015) Micro- and nanomachining. Emerging Nanotechnol Manuf (Second Edition) 202–229
174. Xu ZW, He ZD, Song Y, Fu X, Rommel M, Luo XC, Hartmaier A, Zhang JJ, Fang FZ (2018) Topic Review:Application of Raman Spectroscopy Characterization in Micro/Nano-Machining. Micromachines
175. Bao J, Li L, He N, Cao ZY, Huang L (2009) A brief review of micro-milling Technology. Aerosp Sci Technol
176. Yan Y, Chang SY, Wang T, Geng YQ (2019) Scratch on polymer materials using AFM tip-based approach: a review. Polymers 11(10):1590
177. Jackson MJ, Whitfield MD, Robinson GM, Handy RG, Morrell JS, Ahmed W, Sein H (2015) Micromachining from a Materials Perspective. Springer International Publishing
178. Wang LY, Du XH, Zhang FF, Li AL, Sun DH (2016) Micro/nano fabrication technology of non-silicon material for aeronautical MEMS Systems. Aero Manuf Technol
179. Zhang JH, Tian FQ, Zhang ML, Zhao Y (2016) Review of studies on micro-grinding and ultrasonic-assisted machining. Shock Vib
180. Habrat W, Motyka M, Topolski K, Sieniawski J (2016) Evaluation of the cutting force components and the surface roughness in the milling process of micro-and nanocrystalline titanium. Arch Metall Mater 61(3):1033–1038
181. Wang SM, Chen DF, Jang MC, Tsooj S (2012) Development of micro milling force model and cutting parameter optimization. Trans Nonferrous Met Soc 22:s851-s858
182. Jeon HJ, Lee EH, Yoo HW, Kim KH, Jung HT (2014) Fabrication of sub-20 nm nano-gap structures through the elastomeric nanostamp assisted secondary sputtering phenomenon. Nanoscale 6(11):5953–5959

183. Fang FZ, Lai M (2014) Development of nanometric cutting mechanism. Sci Sinica 44(10):1052
184. Yan YD, Dong S, Sun T (2005) 3D force components measurement in AFM scratching tests. Ultramicroscopy 105(1):62–71
185. Zhang K, Liu GZ, Gao HY, Sun H, Tang YL, Wu YH (2012) Effect of machining parameters on nano-cutting of SiC ceramics. Adv Mater Res 472–475:1069–1073
186. Cai MB, Li XP, Rahman M (2007) Study of the temperature and stress in nanoscale ductile mode cutting of silicon using molecular dynamics simulation. J Mat Process Technol 192 (10) :607–612
187. Goel S, Luo XC, Reuben RL, Rashid WB (2011) Atomistic aspects of ductile responses of cubic silicon carbide during nanometric cutting. Nanoscale Res Lett 6(1):589
188. Zhang JJ, Sun T, Yan YD, Liang YC, Dong S (2009) Molecular dynamics study of groove fabrication process using AFM-based nanometric cutting technique. Appl Phys A 94(3):593–600
189. Tang QH (2007) MD simulation of dislocation mobility during cutting with diamond tip on silicon. Mater Sci Semi Proc 10(6) :270–275
190. Goel S, Luo XC, Reuben RL, Rashid WB (2012) Replacing diamond cutting tools with CBN for efficient nanometric cutting of silicon. Mat Lett 68:507–509
191. Oluwajobi AO, Chen X (2013) Effects of interatomic potentials on the determination of the minimum depth of cut in nanomachining. Int J Abras Technol 6(1):16
192. Li JH, Dai XD, Liang SH, Tai KP, Kong Y, Liu BX (2008) Interatomic potentials of the binary transition metal systems and some applications in materials physics. Phys Rep 455(1–3):1–134
193. Kildishev AV, Boltasseva A, Shalaev VM (2013) Planar Photonics with Meta-surfaces. Science 339(6125):1232009
194. Lafaye S, Troyon M (2006) On the friction behaviour in nanoscratch testing. Wear 261 (7) :905–913
195. Beake BD, Harris AJ, Liskiewicz TW (2013) Review of recent progress in nanoscratch testing. Tribology 7(2):87–96
196. To S, Zhu ZW, Zeng WH (2015) Novel end-fly-cutting-servo system for deterministic generation of hierarchical micro-nanostructures.CIRP Ann Manuf Technol 64 (1) :133–136
197. Tseng AA (2004) Recent developments in micromilling using focused ion beam technology. J Micromech Microeng 14(14):15–34
198. Berg RVD (2005) Extreme UV Lithography Preserves Moore's Law. Optics & Laser Europe 129:29–31
199. Ru CH, Luo J, Xie SR, Sun Y (2014) A review of non-contact micro- and nano-printing technologies. J Micromech Microeng 24(5):053001
200. Pimpin A, Srituravanich W (2012) Review on micro- and nanolithography techniques and their applications. Engineering Journal 16(1):37–56
201. Qin Y (2010) Overview of Micro-Manufacturing. Micro Manuf Eng and Technol
202. Lee YJ, Wang H (2020) Current understanding of surface effects in microcutting. Mater and Des 192: 108688
203. Xie WK, Fang FZ (2020) Mechanism of atomic and close-to-atomic scale cutting of monocrystalline copper. App Surf Sci 503:144239